arXiv:1406.4143v1 [astro-ph.CO] 16 Jun 2014

The One-Loop Matter Bispectrum in the Effective Field Theory of Large Scale Structures

Raul E. Angulo[1], Simon Foreman[2,3],

Marcel Schmittfull[4], and Leonardo Senatore[2,3]

[1] *Centro de Estudios de Fisica del Cosmos de Aragon, Plaza San Juan 1, Planta-2, 44001, Teruel, Spain*

[2] *Stanford Institute for Theoretical Physics and Department of Physics, Stanford University, Stanford, CA 94306*

[3] *Kavli Institute for Particle Astrophysics and Cosmology, SLAC and Stanford University, Menlo Park, CA 94025*

[4] *Berkeley Center for Cosmological Physics, Department of Physics, University of California Berkeley and Lawrence Berkeley National Laboratory, Berkeley, CA 94720*

Abstract

Given the importance of future large scale structure surveys for delivering new cosmological information, it is crucial to reliably predict their observables. The Effective Field Theory of Large Scale Structures (EFTofLSS) provides a manifestly convergent perturbative scheme to compute the clustering of dark matter in the weakly nonlinear regime in an expansion in $k/k_{\rm NL}$, where k is the wavenumber of interest and $k_{\rm NL}$ is the wavenumber associated to the nonlinear scale. It has been recently shown that the EFTofLSS matches to 1% level the dark matter power spectrum at redshift zero up to $k \simeq 0.3h\,{\rm Mpc}^{-1}$ and $k \simeq 0.6h\,{\rm Mpc}^{-1}$ at one and two loops respectively, using only one counterterm that is fit to data. Similar results have been obtained for the momentum power spectrum at one loop. This is a remarkable improvement with respect to former analytical techniques. Here we study the prediction for the equal-time dark matter bispectrum at one loop. We find that at this order it is sufficient to consider the same counterterm that was measured in the power spectrum. Without any remaining free parameter, and in a cosmology for which $k_{\rm NL}$ is smaller than in the previously considered cases, we find that the prediction from the EFTofLSS agrees very well with N-body simulations up to $k \simeq 0.3h\,{\rm Mpc}^{-1}$, given the accuracy of the measurements, which is of order a few percent at the highest k's of interest. While the fit is very good on average up to $k \simeq 0.3h\,{\rm Mpc}^{-1}$, the fit performs slightly worse on equilateral configurations, failing approximately at $k \simeq 0.23h\,{\rm Mpc}^{-1}$, in agreement with expectations that for a given maximum k, equilateral triangles are the most nonlinear.

Contents

1 Introduction **2**

2 Formulas for One-Loop EFT Prediction **4**
2.1 The IR-Safe Integrand of $B_{\text{1-loop}}$ 4
2.2 Counterterms 8

3 Comparison with Simulations **11**
3.1 N-body simulations 11
3.1.1 Bispectrum and estimation of errors 12
3.2 Determining $c^2_{s(1)}$ from the matter power spectrum 12
3.3 Bispectrum results 14

4 Conclusions **18**

A Solving the Equations of Motion **20**
A.1 Loop corrections and linear counterterms 20
A.2 Quadratic counterterms 24

B Divergences and Renormalization in Scaling Universes **25**

C A Simplification to the IR Resummation **27**

D Consistency Check using Other Simulations **28**

1 Introduction

To explore the dynamics that drove the inflationary period, it is necessary to probe a large number of modes. The upcoming release of the polarization data from the Planck satellite will increase the amount of available data by at most a factor of two, which means that our knowledge of inflation will be improved by a similar amount, depending on the quantity being constrained. After this, no significant increase in the number of available modes is expected from the CMB, even though some high-ℓ measurement might still contain some interesting information. Notice that this situation applies quite unaltered also in the case in which the recent claimed discovery of primordial B modes from the BICEP experiment [1] is confirmed. Such a measurement would indeed imply a discovery that Inflation happened at high energies, but it would not enlighten us in detail on the dynamics that drove inflation, for which we need more modes.

This tells us that it is crucial for the field of cosmology to find ways of accessing more primordial modes. The best option to find more modes in the next decade is from large scale structure (LSS) surveys. It is still unclear how many modes will contain relevant cosmological information, and in particular how many of these modes will be accessible with analytical techniques. In order to address

this question, the Effective Field Theory of Large Scale Structures (EFTofLSS) was developed in [2, 3]. The EFTofLSS is different from all former available approaches, such as SPT [4] or RPT [5], for the fact that it acknowledges that analytical predictions cannot be made to arbitrarily small scales where the dynamics is completely nonlinear. The effect of short scales on long modes is encapsulated in a series of terms in the equations of motion of the long modes, whose numerical coefficients are not known, and need to be fitted to data or to N-body simulations. The role of these additional terms is to compensate for any erroneous dependence on short distance physics that appears when performing calculations in perturbation theory. This is what, in the context of particle physics, goes under the name of renormalization, which is why these additional terms that appear in the equations of motion are often referred to as counterterms.

As described in [6, 7], after the inclusion of these counterterms and after renormalization, perturbation theory amounts to an expansion in the parameters: $\epsilon_{\delta<}$ and $\epsilon_{s>}$. These are defined as

$$\epsilon_{s>} = k^2 \int_k^\infty \frac{d^3k'}{(2\pi)^3} \frac{P_{11}(k')}{k'^2} \ , \qquad (1)$$
$$\epsilon_{\delta<} = \int_0^k \frac{d^3k'}{(2\pi)^3} P_{11}(k') \ ,$$

where $P_{11}(k)$ is the dark matter power spectrum. $\epsilon_{\delta<}$ represents the effect of tidal forces on a given region, while $\epsilon_{s>}$ accounts for the short distance displacements. Both of these scale proportionally to powers of $k/k_{\rm NL}$, where $k_{\rm NL}$ is the wavenumber associated to the nonlinear scale. In the most common treatment, the so-called Eulerian one, we expand also in the effect of the long distance displacements $\epsilon_{s<} = (k\,\delta s_<)^2$, where

$$\epsilon_{s_<} \ = \ k^2 \int_0^k \frac{d^3k'}{(2\pi)^3} \frac{P_{11}(k')}{k'^2} \ . \qquad (2)$$

As described in [7], it is not possible in general to expand in $\epsilon_{s_<}$, as for the modes of interest this parameter is of order one in our universe. However, there are some quantities, so called IR-safe, for which the effect of $\epsilon_{s_<}$ almost cancels out completely, leaving only a small 2% effect connected to the Baryon Acoustic Oscillations. In general, to deal with the effects related to $\epsilon_{s_<}$, a resummation of the IR-modes needs to be performed, as it was done in [7]. After this is done, the expansion parameters in the EFTofLSS remain only $\epsilon_{s_>}$ and $\epsilon_{\delta<}$, which are smaller than one for $k \lesssim k_{\rm NL}$. This means that, apart for non-perturbative effects that dominate at very small distances, perturbation theory with the EFTofLSS is manifestly convergent.

So far, the EFTofLSS has been used to predict the power spectrum of dark matter at redshift zero. The results have been incredibly encouraging. The results at two loops [8], after IR resummation [7], agree at 1% with N-body simulations to the remarkably high wavenumber of $k \simeq 0.6h\,{\rm Mpc}^{-1}$. This represents an improvement of about a factor of six in wavenumber with respect to former analytic techniques, such as SPT. Since available modes scale as the cube of the maximum wavenumber that can be predicted, $k^3_{\rm max}$, these results tell us that there is potentially a factor of about 200 more modes that are amenable to an analytic treatment in next generation LSS surveys than previously

believed. Such a potentially picture-changing result makes it very important to check if a comparable improvement persists for every observable. In [7], the momentum power spectrum, which is not an IR-safe quantity, was computed at one loop, where it was shown that, without the need of fitting any additional parameter, the prediction for the momentum showed a gain in the UV reach that was comparable to the one seen for the matter power spectrum, with percent agreement up to $k \simeq 0.3h\,\mathrm{Mpc}^{-1}$. At this point it is tempting to see if a similar improvement holds for higher n-point functions. The easiest one is the bispectrum at one-loop, which is the subject of study of this paper.

2 Formulas for One-Loop EFT Prediction

We wish to obtain a prediction for the matter bispectrum $B(k_1, k_2, k_3)$, defined by

$$\langle \delta(\boldsymbol{k}_1)\delta(\boldsymbol{k}_2)\delta(\boldsymbol{k}_3)\rangle = (2\pi)^3\delta_{\mathrm{D}}(\boldsymbol{k}_1+\boldsymbol{k}_2+\boldsymbol{k}_3)B(k_1,k_2,k_3)\ , \tag{3}$$

where the Dirac delta function δ_{D} is written with a subscript to distinguish it from the matter overdensity δ. Note that, by translation and rotation invariance, the bispectrum is a function of the magnitudes of three wavevectors that add to form a triangle in momentum space, and does not depend on the specific orientation of the triangle. The bispectrum also depends on the time of observation, but in this work we are only concerned with the predictions at $z = 0$, so we will suppress the time-dependence in what follows.

App. A reviews the generic method for solving the equations of motion for δ and the velocity field v^i and thereby deriving expressions for their correlation functions, and also defines the relevant notation for the solutions (most of which will be familiar from the literature involving SPT, e.g. [4]). Using the procedure outlined in this appendix, and also described in [8] (see also [2]), the lowest-order expression for the bispectrum, which we call B_{tree} because it is a tree graph if written out diagrammatically, is found to be

$$B_{\mathrm{tree}}(k_1,k_2,k_3) = 2P_{11}(k_1)P_{11}(k_2)F_2^{(\mathrm{s})}(\boldsymbol{k}_1,\boldsymbol{k}_2) + 2 \text{ permutations}\ , \tag{4}$$

where $P_{11}(k)$ is the linear matter power spectrum. The next-order corrections to this expression are the one-loop SPT diagrams $B_{\text{1-loop}}$, discussed in Sec. 2.1, and various counterterms arising from the terms in the effective stress tensor, which have not previously been included in bispectrum calculations and which we discuss in Sec. 2.2.

2.1 The IR-Safe Integrand of $B_{\text{1-loop}}$

The one-loop correction in SPT is commonly written as the sum of four terms (e.g. [9]):

$$B_{\text{1-loop}} = B_{222} + B_{321}^{(\mathrm{I})} + B_{321}^{(\mathrm{II})} + B_{411}\ , \tag{5}$$

where

$$B_{222}(k_1,k_2,k_3) = 8\int_{\boldsymbol{q}} P_{11}(q)P_{11}(|\boldsymbol{k}_2-\boldsymbol{q}|)P_{11}(|\boldsymbol{k}_3+\boldsymbol{q}|) \times F_2^{(\mathrm{s})}(-\boldsymbol{q},\boldsymbol{k}_3+\boldsymbol{q})F_2^{(\mathrm{s})}(\boldsymbol{k}_3+\boldsymbol{q},\boldsymbol{k}_2-\boldsymbol{q})F_2^{(\mathrm{s})}(\boldsymbol{k}_2-\boldsymbol{q},\boldsymbol{q}) \ , \tag{6}$$

$$B_{321}^{(\mathrm{I})}(k_1,k_2,k_3) = 6P_{11}(k_3)\int_{\boldsymbol{q}} P_{11}(q)P_{11}(|\boldsymbol{k}_2-\boldsymbol{q}|) \times F_3^{(\mathrm{s})}(-\boldsymbol{q},-\boldsymbol{k}_2+\boldsymbol{q},-\boldsymbol{k}_3)F_2^{(\mathrm{s})}(\boldsymbol{q},\boldsymbol{k}_2-\boldsymbol{q}) + 5 \text{ permutations} \ , \tag{7}$$

$$B_{321}^{(\mathrm{II})}(k_1,k_2,k_3) = 6P_{11}(k_2)P_{11}(k_3)F_2^{(\mathrm{s})}(\boldsymbol{k}_2,\boldsymbol{k}_3)\int_{\mathrm{q}} P_{11}(q)F_3^{(\mathrm{s})}(\boldsymbol{k}_3,\boldsymbol{q},-\boldsymbol{q}) + 5 \text{ permutations} \ , \tag{8}$$

$$B_{411}(k_1,k_2,k_3) = 12P_{11}(k_2)P_{11}(k_3)\int_{\boldsymbol{q}} P_{11}(q)F_4^{(\mathrm{s})}(\boldsymbol{q},-\boldsymbol{q},-\boldsymbol{k}_2,-\boldsymbol{k}_3) + 2 \text{ permutations} \tag{9}$$

and we have used $\int_{\boldsymbol{q}} \equiv \int \frac{d^3q}{(2\pi)^3}$. However, as described in [10], explicitly for the case of loop corrections to the power spectrum, it is possible and indeed very convenient to group these terms together as a single integrand to avoid possible numerical issues in the evaluation of the integral. They arise from large IR contributions in each diagram that, for IR-safe quantities, cancel in the final answer. To accomplish this, we first need to map each potential IR divergence in momentum space to the origin ($\boldsymbol{q}=0$). These divergences are located at points where the argument of a factor of P_{11} can approach zero, keeping the external momenta fixed at some nonzero values.

In $B_{321}^{(\mathrm{II})}$ and B_{411}, the only point where this can occur is $\boldsymbol{q}\to 0$, so no re-mapping is necessary. In $B_{321}^{(\mathrm{I})}$, if we examine the first permutation of external momenta that is explicitly written above, there are potential divergences at $\boldsymbol{q}\to 0$ and $\boldsymbol{q}\to\boldsymbol{k}_2$; the second point can be mapped to the first one by the following manipulation, where $b_{321}^{(\mathrm{I})}(\boldsymbol{q})$ (which also depends on the external momenta, but we suppress that dependence here) refers to the integrand of $B_{321}^{(\mathrm{I})}$:

$$\begin{aligned}\int_{\boldsymbol{q}} b_{321}^{(\mathrm{I})}(\boldsymbol{q}) &= \int_{q<|\boldsymbol{k}_2-\boldsymbol{q}|}\frac{d^3q}{(2\pi)^3}b_{321}^{(\mathrm{I})}(\boldsymbol{q}) + \int_{q>|\boldsymbol{k}_2-\boldsymbol{q}|}\frac{d^3q}{(2\pi)^3}b_{321}^{(\mathrm{I})}(\boldsymbol{q}) \\ &= \int_{q<|\boldsymbol{k}_2-\boldsymbol{q}|}\frac{d^3q}{(2\pi)^3}b_{321}^{(\mathrm{I})}(\boldsymbol{q}) + \int_{\tilde{q}<|\boldsymbol{k}_2-\tilde{\boldsymbol{q}}|}\frac{d^3\tilde{q}}{(2\pi)^3}b_{321}^{(\mathrm{I})}(\boldsymbol{k}_2-\tilde{\boldsymbol{q}}) \\ &= 2\int_{q<|\boldsymbol{k}_2-\boldsymbol{q}|}\frac{d^3q}{(2\pi)^3}b_{321}^{(\mathrm{I})}(\boldsymbol{q}) = 2\int_{\boldsymbol{q}} b_{321}^{(\mathrm{I})}(\boldsymbol{q})\,\Theta(|\boldsymbol{k}_2-\boldsymbol{q}|-q) \ ,\end{aligned} \tag{10}$$

where we have used the symmetry of $b_{321}^{(\mathrm{I})}(\boldsymbol{q})$ under the substitution $\boldsymbol{q}\to\boldsymbol{k}_2-\boldsymbol{q}$. An analogous manipulation must be applied to each of the other 5 permutations of external momenta.

The case of B_{222} is more complicated, for two reasons. The first is the fact that divergences can occur at three locations ($\boldsymbol{q}\to 0$, $\boldsymbol{q}\to\boldsymbol{k}_2$, and $\boldsymbol{q}\to-\boldsymbol{k}_3$), and the last two must be mapped to the first one. The second is that the form of B_{222} written in Eq. (6) is proportional to $P_{11}(k_2)P_{11}(k_3)$ in the $\boldsymbol{q}\to 0$ limit of the integral, while there are permutations of the other terms that will be

proportional to $P_{11}(k_1)$ in this limit. Since the IR limits of each integral must cancel with each other regardless of the form of P_{11}, this means that we might expect to have to manipulate B_{222} to produce terms proportional to $P_{11}(k_1)$, in addition to re-mapping the divergences mentioned above.

Fortunately, these manipulations proceed in a fairly straightforward way. First, let us multiply the integrand of B_{222} by a sum of products of step functions, like so:

$$\begin{aligned} B_{222}(k_1,k_2,k_3) = 8\int_{\boldsymbol{q}} & P_{11}(q)P_{11}(|\boldsymbol{k}_2-\boldsymbol{q}|)P_{11}(|\boldsymbol{k}_3+\boldsymbol{q}|) \\ & \times F_2^{(\mathrm{s})}(-\boldsymbol{q},\boldsymbol{k}_3+\boldsymbol{q})F_2^{(\mathrm{s})}(\boldsymbol{k}_3+\boldsymbol{q},\boldsymbol{k}_2-\boldsymbol{q})F_2^{(\mathrm{s})}(\boldsymbol{k}_2-\boldsymbol{q},\boldsymbol{q}) \\ & \times \left[\Theta(|\boldsymbol{k}_2-\boldsymbol{q}|-q)\left\{\Theta(|\boldsymbol{k}_3+\boldsymbol{q}|-q)+\Theta(q-|\boldsymbol{k}_3+\boldsymbol{q}|)\right\}\right. \\ & \quad \left. +\Theta(q-|\boldsymbol{k}_2-\boldsymbol{q}|)\left\{\Theta(|\boldsymbol{k}_3+\boldsymbol{q}|-q)+\Theta(q-|\boldsymbol{k}_3+\boldsymbol{q}|)\right\}\right] \ . \end{aligned} \tag{11}$$

We can now split the integrand into four terms, each multiplying a different product of step functions, and manipulate them so that each term has potential IR divergences only as $\boldsymbol{q}\to 0$:

1. $\underline{\Theta(|\boldsymbol{k}_2-\boldsymbol{q}|-q)\Theta(|\boldsymbol{k}_3+\boldsymbol{q}|-q)}$:
   As $\boldsymbol{q}\to\boldsymbol{k}_2$ or $\boldsymbol{q}\to-\boldsymbol{k}_3$, these step functions evaluate to zero, and therefore this term requires no further manipulation.

2. $\underline{\Theta(|\boldsymbol{k}_2-\boldsymbol{q}|-q)\Theta(q-|\boldsymbol{k}_3+\boldsymbol{q}|)}$:
   This term is zero when $\boldsymbol{q}\to\boldsymbol{k}_2$, but not when $\boldsymbol{q}\to-\boldsymbol{k}_3$. However, if we let $\boldsymbol{q}=-\boldsymbol{k}_3-\tilde{\boldsymbol{q}}$, then the integrand becomes

   $$\begin{aligned} & 8P_{11}(|\boldsymbol{k}_3+\tilde{\boldsymbol{q}}|)P_{11}(|-\boldsymbol{k}_1+\tilde{\boldsymbol{q}}|)P_{11}(\tilde{q})F_2^{(\mathrm{s})}(\boldsymbol{k}_3+\tilde{\boldsymbol{q}},-\tilde{\boldsymbol{q}})F_2^{(\mathrm{s})}(-\tilde{\boldsymbol{q}},-\boldsymbol{k}_1+\tilde{\boldsymbol{q}})F_2^{(\mathrm{s})}(-\boldsymbol{k}_1+\tilde{\boldsymbol{q}},-\tilde{\boldsymbol{q}}) \\ & \quad \times\Theta(|-\boldsymbol{k}_1+\tilde{\boldsymbol{q}}|-|\boldsymbol{k}_3+\tilde{\boldsymbol{q}}|)\Theta(|\boldsymbol{k}_3+\tilde{\boldsymbol{q}}|-\tilde{q}) \ , \end{aligned} \tag{12}$$

   which has potential singularities at $\tilde{\boldsymbol{q}}\to\boldsymbol{k}_1$ and $\tilde{\boldsymbol{q}}\to-\boldsymbol{k}_3$, but the step functions evaluate to zero in these limits.

3. $\underline{\Theta(q-|\boldsymbol{k}_2-\boldsymbol{q}|)\Theta(|\boldsymbol{k}_3+\boldsymbol{q}|-q)}$:
   This term is zero when $\boldsymbol{q}\to-\boldsymbol{k}_3$, but not when $\boldsymbol{q}\to\boldsymbol{k}_2$, but the substitution $\boldsymbol{q}=\boldsymbol{k}_2-\tilde{\boldsymbol{q}}$ changes the integrand to

   $$\begin{aligned} & 8P_{11}(|\boldsymbol{k}_2-\tilde{\boldsymbol{q}}|)P_{11}(\tilde{q})P_{11}(|\boldsymbol{k}_1+\tilde{\boldsymbol{q}}|)F_2^{(\mathrm{s})}(-\boldsymbol{k}_2+\tilde{\boldsymbol{q}},-\boldsymbol{k}_1-\tilde{\boldsymbol{q}})F_2^{(\mathrm{s})}(-\boldsymbol{k}_1-\tilde{\boldsymbol{q}},\tilde{\boldsymbol{q}})F_2^{(\mathrm{s})}(\tilde{\boldsymbol{q}},\boldsymbol{k}_2-\tilde{\boldsymbol{q}}) \\ & \quad \times\Theta(|\boldsymbol{k}_2-\tilde{\boldsymbol{q}}|-\tilde{q})\Theta(|\boldsymbol{k}_1+\tilde{\boldsymbol{q}}|-|\boldsymbol{k}_2-\tilde{\boldsymbol{q}}|) \ , \end{aligned} \tag{13}$$

   which again only has potential singularities at $\tilde{\boldsymbol{q}}\to 0$, thanks to the step functions.

4. $\underline{\Theta(q-|\boldsymbol{k}_2-\boldsymbol{q}|)\Theta(q-|\boldsymbol{k}_3+\boldsymbol{q}|)}$:
   After substituting $\boldsymbol{q}=\boldsymbol{k}_2-\tilde{\boldsymbol{q}}$, the integrand is the same in case 3, but with step functions

   $$\Theta(|\boldsymbol{k}_2-\tilde{\boldsymbol{q}}|-\tilde{q})\Theta(|\boldsymbol{k}_2-\tilde{\boldsymbol{q}}|-|\boldsymbol{k}_1+\tilde{\boldsymbol{q}}|) \ , \tag{14}$$

which evaluate to zero as $\tilde{\boldsymbol{q}} \to \boldsymbol{k}_2$, and also for $\tilde{\boldsymbol{q}} \to -\boldsymbol{k}_1$, but only if $k_3 < k_1$. If $k_3 > k_1$, we should repeat the steps above, starting from Eq. (11), but interchanging $\boldsymbol{k}_1$ and $\boldsymbol{k}_3$ and propagating this change through each step. Each of the two cases can then be selected for via appropriate step functions (we will write this explicitly when we present the final $B_{\text{1-loop}}$ expression below).

Thus, we have shown how to write the integrand of B_{222} in a way that the only potential divergence is located at $\boldsymbol{q} \to 0$. Notice also that our manipulations have introduced terms containing $P_{11}(k_1)$ in this limit, which will serve to cancel the corresponding terms appearing when external momenta are permuted in the other diagrams.

While the above procedure takes care of the leading IR divergences, there are still subleading divergences that would normally disappear after integration over orientations of $\boldsymbol{q}$ is carried out. These can be made to cancel prior to integration if an appropriate symmetrization over angles is implemented, but the details of the symmetrization depend on the technique used to translate the integrand into a form that can be evaluated numerically [1].

Thus, the final IR-safe form of $B_{\text{1-loop}}$ can be written in the following way:

$$B_{\text{1-loop}}(k_1,k_2,k_3) = \int_{\boldsymbol{q}} \left[b_{222}^{(k_3>k_1)}\Theta(k_3-k_1) + b_{222}^{(k_3<k_1)}\Theta(k_1-k_3) + b_{321}^{(\text{I})} + b_{321}^{(\text{II})} + b_{411} \right]_{\text{sym. over angles}} , \tag{15}$$

where

$$\begin{aligned}
b_{222}^{(k_3>k_1)} \equiv\ & 8P_{11}(q)P_{11}(|\boldsymbol{k}_2-\boldsymbol{q}|)P_{11}(|\boldsymbol{k}_3+\boldsymbol{q}|)F_2^{(\text{s})}(-\boldsymbol{q},\boldsymbol{k}_3+\boldsymbol{q})F_2^{(\text{s})}(\boldsymbol{k}_3+\boldsymbol{q},\boldsymbol{k}_2-\boldsymbol{q}) \\
& \times F_2^{(\text{s})}(\boldsymbol{k}_2-\boldsymbol{q},\boldsymbol{q})\Theta(|\boldsymbol{k}_2-\boldsymbol{q}|-q)\Theta(|\boldsymbol{k}_3+\boldsymbol{q}|-q) \\
& + 8P_{11}(|\boldsymbol{k}_3+\tilde{\boldsymbol{q}}|)P_{11}(|-\boldsymbol{k}_1+\tilde{\boldsymbol{q}}|)P_{11}(\tilde{q})F_2^{(\text{s})}(\boldsymbol{k}_3+\tilde{\boldsymbol{q}},-\tilde{\boldsymbol{q}})F_2^{(\text{s})}(-\tilde{\boldsymbol{q}},-\boldsymbol{k}_1+\tilde{\boldsymbol{q}}) \\
& \times F_2^{(\text{s})}(-\boldsymbol{k}_1+\tilde{\boldsymbol{q}},-\tilde{\boldsymbol{q}})\Theta(|-\boldsymbol{k}_1+\tilde{\boldsymbol{q}}|-|\boldsymbol{k}_3+\tilde{\boldsymbol{q}}|)\Theta(|\boldsymbol{k}_3+\tilde{\boldsymbol{q}}|-\tilde{q}) \\
& + 8P_{11}(|\boldsymbol{k}_2-\tilde{\boldsymbol{q}}|)P_{11}(\tilde{q})P_{11}(|\boldsymbol{k}_1+\tilde{\boldsymbol{q}}|)F_2^{(\text{s})}(-\boldsymbol{k}_2+\tilde{\boldsymbol{q}},-\boldsymbol{k}_1-\tilde{\boldsymbol{q}})F_2^{(\text{s})}(-\boldsymbol{k}_1-\tilde{\boldsymbol{q}},\tilde{\boldsymbol{q}}) \\
& \times F_2^{(\text{s})}(\tilde{\boldsymbol{q}},\boldsymbol{k}_2-\tilde{\boldsymbol{q}})\Theta(|\boldsymbol{k}_2-\tilde{\boldsymbol{q}}|-\tilde{q})\Theta(|\boldsymbol{k}_1+\tilde{\boldsymbol{q}}|-|\boldsymbol{k}_2-\tilde{\boldsymbol{q}}|) \\
& + 8P_{11}(|\boldsymbol{k}_2-\tilde{\boldsymbol{q}}|)P_{11}(\tilde{q})P_{11}(|\boldsymbol{k}_1+\tilde{\boldsymbol{q}}|)F_2^{(\text{s})}(-\boldsymbol{k}_2+\tilde{\boldsymbol{q}},-\boldsymbol{k}_1-\tilde{\boldsymbol{q}})F_2^{(\text{s})}(-\boldsymbol{k}_1-\tilde{\boldsymbol{q}},\tilde{\boldsymbol{q}}) \\
& \times F_2^{(\text{s})}(\tilde{\boldsymbol{q}},\boldsymbol{k}_2-\tilde{\boldsymbol{q}})\Theta(|\boldsymbol{k}_2-\tilde{\boldsymbol{q}}|-\tilde{q})\Theta(|\boldsymbol{k}_2-\tilde{\boldsymbol{q}}|-|\boldsymbol{k}_1+\tilde{\boldsymbol{q}}|) , \qquad (16) \\
b_{222}^{(k_3<k_1)} \equiv\ & b_{222}^{(k_3>k_1)}\Big|_{\boldsymbol{k}_1\leftrightarrow\boldsymbol{k}_3} , \qquad (17)
\end{aligned}$$

[1] For example, we could choose the z-axis to lie along $\boldsymbol{k}_1$, and make the substitution $\boldsymbol{q} = (q\sqrt{1-\mu^2}\cos(\phi), q\sqrt{1-\mu^2}\sin(\phi), q\mu)$. In this case, there are potentially IR-divergent terms containing $(\boldsymbol{k}_2\cdot\boldsymbol{q})^2$, which itself contains the term $\sim \mu\sqrt{1-\mu^2}\sin(\phi)$. This dangerous term will vanish if the integrand is symmetrized in μ and $-\mu$, but *not* if the symmetrization is over $\boldsymbol{q}$ and $-\boldsymbol{q}$, since this would flip the signs of both μ and $\sin(\phi)$. In our own numerical work, we choose to symmetrize in μ and $-\mu$, and have verified analytically for the case of a scaling universe that all subleading IR divergences cancel as intended when this symmetrization is implemented.

and

$$b_{321}^{(\mathrm{I})} \equiv 12 P_{11}(k_3) P_{11}(q) P_{11}(|\boldsymbol{k}_2 - \boldsymbol{q}|) F_3^{(\mathrm{s})}(-\boldsymbol{q}, -\boldsymbol{k}_2 + \boldsymbol{q}, -\boldsymbol{k}_3) F_2^{(\mathrm{s})}(\boldsymbol{q}, \boldsymbol{k}_2 - \boldsymbol{q}) \times \Theta(|\boldsymbol{k}_2 - \boldsymbol{q}| - q) + 5 \text{ permutations} , \tag{18}$$

$$b_{321}^{(\mathrm{II})} \equiv 6 P_{11}(k_2) P_{11}(k_3) F_2^{(\mathrm{s})}(\boldsymbol{k}_2, \boldsymbol{k}_3) P_{11}(q) F_3^{(\mathrm{s})}(\boldsymbol{k}_3, \boldsymbol{q}, -\boldsymbol{q}) + 5 \text{ permutations} , \tag{19}$$

$$b_{411} \equiv 12 P_{11}(k_2) P_{11}(k_3) P_{11}(q) F_4^{(\mathrm{s})}(\boldsymbol{q}, -\boldsymbol{q}, -\boldsymbol{k}_2, -\boldsymbol{k}_3) + 2 \text{ permutations} . \tag{20}$$

2.2 Counterterms

In the EFTofLSS, the effects of nonlinearities at short distance scales are encapsulated into an effective stress tensor, $(\partial\tau)_{\rho_l}{}^i$, on the right-hand side of the Euler equation.[2] This stress tensor is written as a double expansion in fields and derivatives, consistent with the symmetries that are relevant at the appropriate scales (namely, rotational invariance and the equivalence principle) The various terms in this expansion add extra contributions to the perturbative solutions for δ and v_i, which lead to the appearance of counterterms in expressions for various observables.

As noted in [8, 11], there is no obvious separation of timescales between the evolution of short and long modes of the density and velocity fields, and therefore $(\partial\tau)_{\rho_l}{}^i$ may exhibit significant non-locality in time. This non-locality will manifest itself in counterterms that are evaluated at loop level, such as those appearing in a two-loop calculation of the power spectrum. In the tree-level counterterms that we restrict ourselves to in this work, any non-locality in time will only have a very minor effect. Furthermore, since in [8] we found that nonlinear power spectrum data seem to prefer only a mild degree of non-locality at best, we will comment on where this non-locality might play a role, but in concrete calculations we will take the local-in-time limit for simplicity.

The lowest-order term in the stress tensor is the linear one, which in the local-in-time limit looks like a "speed of sound" term: schematically,

$$(\partial\tau)_{\rho_l}{}^i \supset c_\mathrm{s}^2 \partial^i \partial^2 \phi \sim c_\mathrm{s}^2 \partial^i \delta . \tag{21}$$

At tree-level, this term will contribute two counterterms to the bispectrum (see App. A for details of the derivation), which, when grouped together into a single expression, take the form

$$B_{c_\mathrm{s}}(k_1, k_2, k_3) = 2 P_{11}(k_1) P_{11}(k_2) \tilde{F}_2^{(\mathrm{s})}(\boldsymbol{k}_1, \boldsymbol{k}_2) + 2 \text{ permutations} - 2\bar{c}_1 k_1^2 P_{11}(k_1) P_{11}(k_2) F_2^{(\mathrm{s})}(\boldsymbol{k}_1, \boldsymbol{k}_2) + 5 \text{ permutations} , \tag{22}$$

where $\tilde{F}_2^{(\mathrm{s})}(\boldsymbol{k}_1, \boldsymbol{k}_2)$ is found using the recurrence relations from [8], with a slight modification to allow for a more general time-dependence of the counterterm than was assumed in [8]. $\bar{c}_1$ is related to the

[2] The operator $(\partial\tau)_{\rho_l}{}^i$ is defined by $(\partial\tau)_{\rho_l}{}^i \equiv \rho^{-1} \partial_j \tau^{ij}$, which is the quantity that actually appears in the Euler equation, where τ^{ij} is the form of the stress tensor more commonly seen in standard treatments of fluids. It is somewhat of an arbitrary choice whether to write an expansion for τ^{ij} or $\rho^{-1}\partial_j\tau^{ij}$; we find it more convenient to expand the latter, and for brevity we will sometimes refer to $(\partial\tau)_{\rho_l}{}^i$ as the "stress tensor," although technically this is a mild abuse of terminology.

free parameter $c^2_{s(1)}$ (which also enters into the one-loop EFT prediction for the power spectrum) by $\bar{c}_1 = (2\pi)c^2_{s(1)}/k^2_{\rm NL}$, while $\tilde{F}_2^{(\rm s)}$ is proportional to a different constant $\bar{c}_2$, which itself is equal to $\bar{c}_1$ times some order-one factor related to the severity of the non-locality in time. Unless the non-locality is very severe, this factor will be very close to one, so the assumption of locality in time (for which $\bar{c}_2 = \bar{c}_1$ exactly) will not have a huge effect.

There are also four other possible tree-level counterterms we can write down, arising from the contribution to the effective stress tensor that is quadratic in the fields. Three of the terms arise from operators like $(\partial^2\phi)^2$: schematically, we have

$$\begin{aligned}(\partial\tau)_{\rho_l}{}^i &\supset \partial^i\left[\partial^2\phi\right]^2 + \partial^i\left[\partial^j\partial^k\phi\,\partial_j\partial_k\phi\right] + \partial^i\partial^j\phi\,\partial_j\partial^2\phi \\ &\sim \partial^i\delta^2 + \partial^i\left[\frac{\partial^j\partial^k}{\partial^2}\delta\cdot\frac{\partial_j\partial_k}{\partial^2}\delta\right] + \frac{\partial^i\partial^j}{\partial^2}\delta\cdot\partial_j\delta\ ,\end{aligned} \tag{23}$$

where we used Poisson's equation to trade $\partial^2\phi$ for δ in the second line. Recall that we could also have written a linear counterterm involving the velocity divergence:

$$(\partial\tau)_{\rho_l}{}^i \supset \partial^i(\partial_j v^j)\ , \tag{24}$$

At linear order, we have that $\theta = \partial_i v^i = -\mathcal{H}f\delta$, where $f \equiv \partial\log D_1/\partial\log a$ with $\mathcal{H} = aH$ and D_1 being the linear growth factor. As usual in SPT, we can rewrite the velocity field as (see Eq. (46) for a more detailed discussion)

$$\theta(a,\boldsymbol{k}) \;=\; -\mathcal{H}(a)\,f\,\hat{\theta}\ , \quad \text{where} \quad \hat{\theta}(a,\boldsymbol{k}) = \sum_{n=1}^{\infty}[D_1(a)]^n\theta^{(n)}(\boldsymbol{k})\ . \tag{25}$$

So we define the new counterterm as proportional to

$$(\partial\tau)_{\rho_l}{}^i \supset \partial^i(\hat{\theta}-\delta)\ , \tag{26}$$

which starts at second order in the fluctuations.

These four counterterms take respectively the following form:

$$\begin{aligned}B_{c_1}(k_1,k_2,k_3) &= -2c_1\,k_1^2P_{11}(k_2)P_{11}(k_3) + 2\text{ permutations}\ , \\ B_{c_2}(k_1,k_2,k_3) &= -2c_2\,k_1^2\frac{(\boldsymbol{k}_2\cdot\boldsymbol{k}_3)^2}{k_2^2k_3^2}P_{11}(k_2)P_{11}(k_3) + 2\text{ permutations}\ , \\ B_{c_3}(k_1,k_2,k_3) &= -c_3\,(\boldsymbol{k}_2\cdot\boldsymbol{k}_3)\left[\frac{\boldsymbol{k}_1\cdot\boldsymbol{k}_2}{k_2^2}+\frac{\boldsymbol{k}_1\cdot\boldsymbol{k}_3}{k_3^2}\right]P_{11}(k_2)P_{11}(k_3) + 2\text{ permutations}\ , \\ B_{c_4}(k_1,k_2,k_3) &= -c_4\,k_1^2\,\frac{k_1^4+(k_2^2-k_3^2)^2-2k_1^2(k_2^2+k_3^2)}{7k_2^2\,k_3^2}P_{11}(k_2)P_{11}(k_3) + 2\text{ permutations}\ ,\end{aligned} \tag{27}$$

where $c_1,\ldots,c_4$ are arbitrary coefficients, each expected to be of order $k_{\rm NL}^{-2}$ (there are no factors of (2π) because these counterterms are associated with loop diagrams that do not contain any trivial

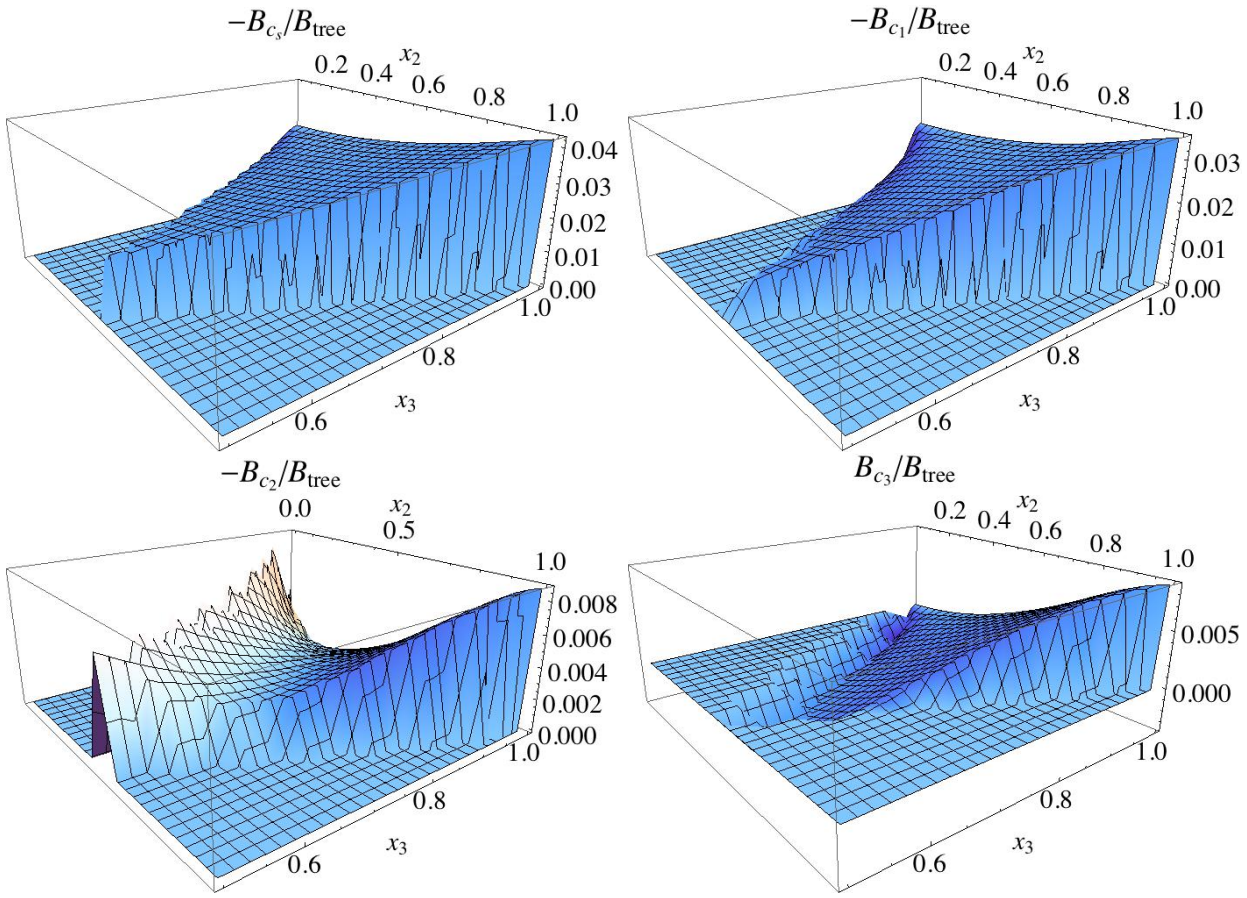

Figure 1: *Ratios of various terms in the bispectrum prediction to the tree-level expression B_{tree}, plotted with $k_1 = 0.1h\,Mpc^{-1}$ and in terms of $x_2 \equiv k_2/k_1$ and $x_3 \equiv k_3/k_1$. To avoid redundancy, we only plot configurations with $x_2 \leq x_3$, while the triangle inequality restricts physical configurations to satisfy $1 - x_3 \leq x_2$. Each term is strongest on equilateral triangles ($x_2 = x_3 = 1$), becoming relatively weaker for other configurations such as squeezed ($x_2 \to 0$) or flat ($x_2 + x_3 = 1$). This implies that configurations where three short modes interact are more nonlinear than configurations involving one or more longer modes and one short mode—in some sense, of all triangles with k_1 fixed, equilateral triangles are "closest" to the nonlinear scale. As we let k_1 grow, all terms grow in size relative to $B_{\rm tree}$ but the shape remains quite unaltered.*

angular integrations). Notice that B_4 is a linear combination of B_1 and B_2

$$B_{c_4}(k_1, k_2, k_3) = -\frac{2}{7} c_4 \left(\frac{B_1(k_1, k_2, k_3)}{c_1} - \frac{B_2(k_1, k_2, k_3)}{c_2} \right) , \tag{28}$$

therefore, since c_1 and c_2 are free parameter, we can neglect B_{c_4} from the rest of the paper.

To gain insight into the effect of these terms on the bispectrum in various configurations, in Fig. 1 we plot the ratio of each counterterm to $B_{\rm tree}$ as a function of $x_2 \equiv k_2/k_1$ and $x_3 \equiv k_3/k_1$ for $k_1 = 0.1h\,{\rm Mpc}^{-1}$ (the scale-dependence of each term is such that these plots do not change

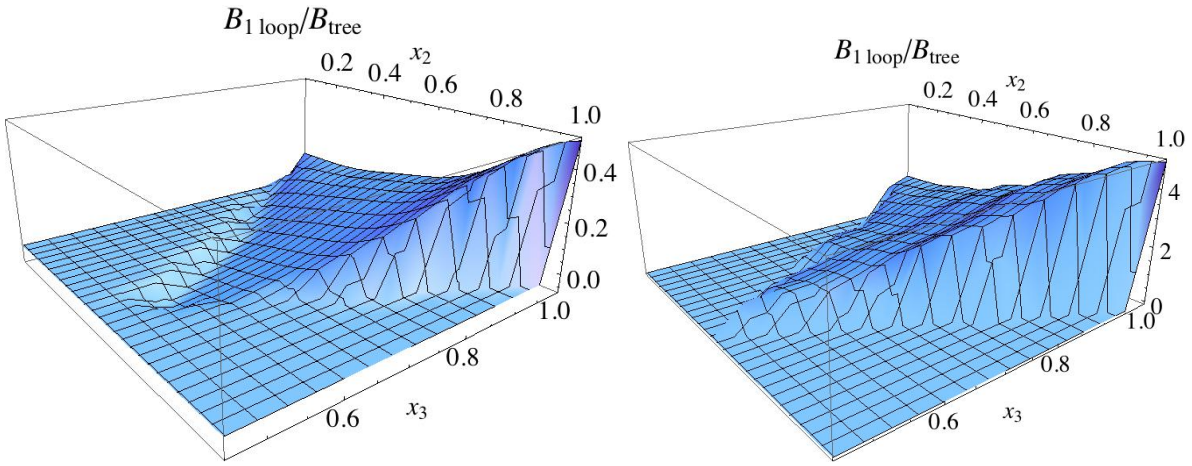

Figure 2: *Same as Fig. 1, but for the 1-loop contribution for $k_1 = 0.1h\,Mpc^{-1}$ on the left and $k_1 = 0.3h\,Mpc^{-1}$ on the right.*

significantly for other values of k_1). In Fig. 2, we show $B_{\text{1-loop}}/B_{\text{tree}}$ for $k_1 = 0.1h\,\text{Mpc}^{-1}$ and $0.3h\,\text{Mpc}^{-1}$. To restrict to physical triangles and avoid redundancy in the plots, we only plot in the range $1 - x_3 < x_2 < x_3$. We see from these plots that each term is strongest for equilateral triangles ($x_2 = x_3 = 1$), and they each become less important for squeezed ($x_3 \approx 1$, $x_2 \approx 0$) and flat ($x_2 + x_3 \approx 1$) configurations (except for B_{c_2}, which tends to peak somewhat in the flat limit). This matches our intuition that of all triangles with one side fixed, equilateral triangles are the most nonlinear, because they are the ones for which each side is closest to the nonlinear scale.

In App. B we show that in the case in which the universe is described by a simple power law, these three counterterms are required to ensure that UV divergences can be cancelled in the bispectrum. This is a sufficient but non-necessary condition that tells that these counterterms should be present in the EFT. It is not a necessary condition because even if these terms were not needed to cancel any UV divergence, they would still be allowed by the symmetry of the problem and therefore should be included.

3 Comparison with Simulations

3.1 N-body simulations

We compare the predictions of the EFTofLSS against the results of a dark-matter only N-body simulation. We use the Millennium-XXL (MXXL) simulation [12], which evolved 6720^3 particles inside a comoving cubical region of $L_{\text{box}} = 3000\,h^{-1}\,\text{Mpc}$ a side, from $z = 63$ to the present day. The combination of a large volume with a high mass resolution of the MXXL suppresses the effects of cosmic variance and discreteness noise in the bispectrum estimates, therefore allowing a detailed comparison with EFT predictions.

The MXXL simulation was carried out with the following set of cosmological parameters: a matter density of $\Omega_{\rm m} = 0.25$ in units of the critical density, a cosmological constant with $\Omega_\Lambda = 0.75$, a Hubble constant $h = 0.73$ in units of $100\,{\rm km\,s^{-1}Mpc^{-1}}$, a spectral index $n_s = 1$ and a normalization parameter $\sigma_8 = 0.9$ for the primordial linear density power spectrum. The initial linear theory power spectrum was computed using the Boltzmann code CAMB [13]. Exactly the same power spectrum and cosmological parameters were used in our EFT calculations.

3.1.1 Bispectrum and estimation of errors

In this paper we focus on the bispectrum of the nonlinear mass density contrast at $z = 0$. In order to compute this quantity we first construct a density field by assigning simulation particles onto a cubic grid using a"cloud-in-cells" deposit scheme. We employ a grid of 1024^3 points and then Fast Fourier Transform the respective density field. Finally, we correct for the effects of the assignment scheme by dividing each Fourier mode by the Fourier transform of a cubical top-hat window.

The power spectrum is computed by spherically averaging the amplitude of Fourier modes in annuli of radius δk. The bispectrum, $B(k_1, k_2, \theta)$, is obtained by performing a nested loop over all grid points (1024^6) and averaging $\delta(k_1)\delta(k_2)\delta(k_3)$ over triangles whose sides satisfy the following condition: $k_1^i = k_1 \pm \frac{1}{2}\delta k$, $k_2^i = k_2 \pm \frac{1}{2}\delta k$ and $\theta^i = \theta \pm \frac{1}{2}\delta\theta$, where $\theta^i = \cos^{-1}\left(\hat{k}_1^i \cdot \hat{k}_2^i\right)$. We note that in subsequent comparisons we discard the imaginary part of the measured bispectrum, and consider only the real one. For these calculations we set $\delta k = 2\pi/L_{\rm box} = 0.0021\,h^{-1}{\rm Mpc}$, and $\delta\theta = \pi/20$.

To close this section we discuss the estimation of the error in the measurement of the bispectrum. We adopt the commonly-used expression derived by [14, 15, 9, 16]:

$$[\Delta B(k_1, k_2, \theta)]^2 = \left(\frac{2\pi}{L_{\rm box}}\right)^3 \frac{s_{123}}{n_{\rm triangles}} P_{\rm NL}(k_1) P_{\rm NL}(k_2) P_{\rm NL}(k_3)\ . \tag{29}$$

This formula is derived in the Gaussian limit, where $P_{\rm NL}$ should be replaced by P_{11}, but it seems to be a better approximation for the scales we are interested in here to replace it with $P_{\rm NL}$. In this expression: s_{123} is equal to 6, 2, 1 for equilateral, isosceles and general triangles, respectively; $n_{\rm triangles}$ is the number of triangles contributing to a given configuration, which, in our case, is directly counted inside the bispectrum code; and $k_3^2 = k_1^2 + k_2^2 - 2k_1k_2\cos(\theta)$. On top of this error, we add an extra 2% error for each bispectrum data point, to account for possible systematic errors in the simulation.

3.2 Determining $c^2_{s(1)}$ from the matter power spectrum

The one-loop EFT prediction for the bispectrum will involve the parameter $c^2_{s(1)}$, which can be determined by fitting the one-loop power spectrum prediction to nonlinear data. As discussed in [2, 8, 7], the one-loop power spectrum in the EFTofLSS takes the form

$$P_{\text{EFT-1-loop}} = P_{11} + P_{\text{1-loop}} - 2\,(2\pi) c^2_{s(1)} \frac{k^2}{k^2_{\rm NL}} P_{11}\ , \tag{30}$$

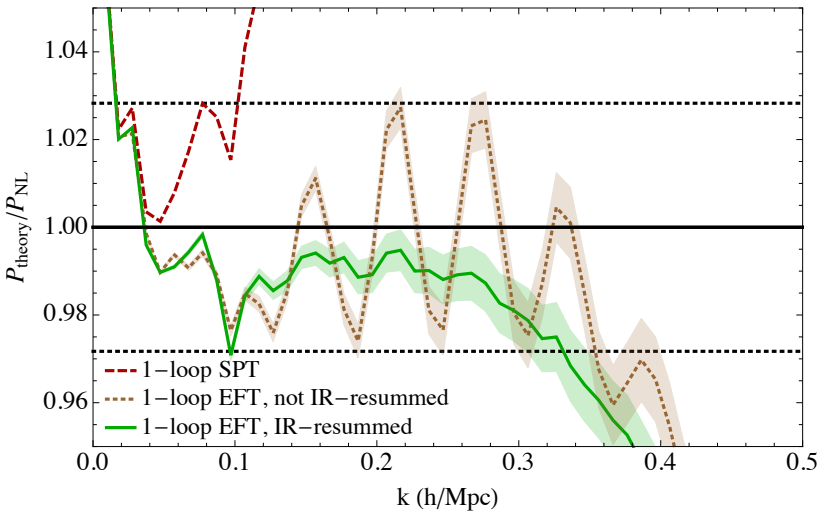

Figure 3: *One-loop SPT and EFT predictions for the matter power spectrum, normalized to measurements from the simulations described in Sec. 3.1. The parameter $c^2_{s(1)}$ in the EFT prediction has been determined by fitting the non-IR-resummed curve over the range $0.15h\,Mpc^{-1} \leq k \leq 0.3h\,Mpc^{-1}$, or equivalently asking the IR-resummed curve to follow horizontally the nonlinear data. The resulting value for $c^2_{s(1)}$ can then be used in the EFT prediction for the bispectrum, without re-fitting. The dashed line correspond to an assumed 2% systematic error in the simulations, added in quadrature with a 2% accuracy goal for the prediction.*

and is expected to be a valid match to the data out to $k \sim 0.3h\,\mathrm{Mpc}^{-1}$, beyond which the two-loop contribution is estimated to become non-negligible. By fitting Eq. (30) to the power spectrum measured from the simulations described in Sec. 3.1, in the k-range $0.15 - 0.3\,h\,\mathrm{Mpc}^{-1}$ [3], we find

$$c^2_{s(1)} = (2.45 \pm 0.07) \times \frac{1}{2\pi}\left(\frac{k_{\rm NL}}{h\,\mathrm{Mpc}^{-1}}\right)^2 \qquad (1\text{-}\sigma). \tag{31}$$

This value is larger than what was obtained from the fits in [8] due to differences in the cosmological model we are fitting to. In particular, [8] used a cosmology with $\sigma_8 \approx 0.8$, while here we have $\sigma_8 \approx 0.9$, so it makes sense that the nonlinearities parametrized by $c^2_{s(1)}$ will be stronger here than in the other paper.

The results of the fit are shown in Fig. 3. The error on $P_{\rm NL}$ due to sampling variance is sub-percent for $k \gtrsim 0.1h\,\mathrm{Mpc}^{-1}$, but we also place uniform 2% errorbars on the data to account for possible systematic errors in the simulation. As in [8], there are residual oscillations of ∼2% around the nonlinear data. These oscillations are due to the effects of bulk flows, and can be eliminated by an appropriate resummation of IR modes, as described in detail in [7] [4] and shown in green in the same figure [5].

[3] As described in [2, 8, 7] the numerical value we obtain for $c^2_{s(1)}$ is quite insensitive to the chosen k-range of the fit.

[4] We find a way to simplify slightly the numerical implementation of the techniques in [7]. We describe it in App. C.

[5] There seems to be a slight systematic offset between the simulation data and the IR-resummed EFT prediction.

3.3 Bispectrum results

In order to utilize the EFTofLSS to make a prediction about the matter bispectrum (or, indeed, any observable), one should have some way of determining which loop corrections and counterterms should be included to reach a given accuracy goal. In [8], estimates were made about the sizes of various terms by treating them in the scaling universe approximation, with $k_{\rm NL}$ and the tilt of the linear power spectrum fit over the range in which the prediction was being made.

We can perform a similar exercise for the bispectrum, in order to estimate when the two-loop correction might become important. The most efficient way to do so is to determine which diagram will have the largest contribution, and then estimate its size. This diagram will arise from the correlator $\left\langle \delta^{(3)}\delta^{(3)}\delta^{(2)} \right\rangle$, and will scale in the following way when evaluated on equilateral configurations:

$$B_{332} \sim \frac{48}{3!\,3!\,2!}(2\pi)^2 \left(\frac{k}{k_{\rm NL}}\right)^{2(3+n)} B_{\rm tree} \ . \tag{32}$$

The $(2\pi)^2$ arises from the fact that this diagram contains two loop integrals that are not nested, which each contribute a factor of (2π) (in the language of [8], it is a "reducible" diagram). The 48 is a combinatoric factor related to the number of ways to sew together the diagram's internal lines, while the factorials in the denominator arise from integrals over Green's functions in time: one can consider the Einstein de-Sitter case, when these Green's functions are roughly the scale factor a, and each factor of $\delta^{(m)}$ will involve m integrals over these factors, yielding a final prefactor of $\sim 1/m!$. The power of $(k/k_{\rm NL})^{(3+n)}$ counts the number of loops, where n is the approximate tilt of P_{11} in the region we're making predictions for.

Other two-loop diagrams can be estimated in the same fashion, but they will all either have fewer factors of (2π) or else will be more strongly suppressed by inverse factorial factors (for which the combinatorics cannot compensate). We should compare this estimate to $B_{\text{EFT-1-loop}}$, which we write as $B_{\rm tree} + B_{\text{1-loop}} + B_{c_s}$. We approximate $B_{\text{1-loop}}$ by the size of its largest diagrams, which come from $\left\langle \delta^{(4)}\delta^{(1)}\delta^{(1)} \right\rangle$:

$$B_{\text{1-loop}} \sim B_{411} \sim \frac{16}{4!}(2\pi) \left(\frac{k}{k_{\rm NL}}\right)^{3+n} B_{\rm tree} \ . \tag{33}$$

Similarly for B_{c_s} we take

$$B_{c_s} \sim 2(2\pi) c^2_{s(1)} \frac{k^2}{k^2_{\rm NL}} B_{\rm tree} \ . \tag{34}$$

To apply these estimates to the universe simulated in Sec. 3.1, we fit a scaling universe power spectrum to the linear spectrum corresponding to the simulations, and find that over the range $0.25h\,\text{Mpc}^{-1} \lesssim k \lesssim 0.60h\,\text{Mpc}^{-1}$, $P_{11}(k) \approx \frac{(2\pi)^3}{k^3_{\rm NL}} \left(\frac{k}{k_{\rm NL}}\right)^n$ with $n \approx -2.1$ and $k_{\rm NL} \approx 3.2h\,\text{Mpc}^{-1}$. Therefore, at $k \sim 0.3h\,\text{Mpc}^{-1}$,

$$\frac{B_{\text{2-loop}}}{B_{\rm tree} + B_{\text{1-loop}} + B_{c_s}} \sim 0.2 \ . \tag{35}$$

This is a very small, quite inconsequential, effect, of about 1% in size, whose origin is hard to investigate. We leave this to future work.

This estimate is uncertain up to $\mathcal{O}(1)$ factors, but it nevertheless indicates that $B_{\text{2-loop}}$ may strongly limit how far into the UV our prediction can reach. Note that the same estimate applied to the universe from [8], which has a more realistic normalization of the power spectrum and hence a more realistic value of k_{NL}, gives 0.1 instead of 0.2, implying that in the real universe, the reach of the prediction should be farther than what it is in this paper.

Alternatively, we can to take a more "experimental" approach, examining the one-loop prediction with all possible counterterms that could appear at this order, and using this to get an idea about where higher-order corrections become important. With three possible counterterms (plus B_{c_s}, whose associated coefficient $c^2_{s(1)}$ is fixed by fitting to the measured nonlinear power spectrum), it is reasonable to think that there might be a risk of over-fitting. However, we find that there is no such risk. We fit the coefficients c_1, c_2, and c_3 in one-loop EFT prediction, given by

$$B_{\text{EFT-1-loop}} = B_{\text{tree}} + B_{\text{1-loop}} + B_{c_s} + B_{c_1} + B_{c_2} + B_{c_3} \ , \tag{36}$$

to measurements of the nonlinear bispectrum from simulations, using all triangles with maximum side length less than some k_{max}. To assess the goodness of fit, we calculate a χ^2 statistic,

$$\chi^2(k_{\text{comp}}) = \sum_{\Delta_i} \frac{(B_{\text{data}}(\Delta_i) - B_{\text{EFT-1-loop}}(\Delta_i)^2)}{\sigma_i^2} \ , \tag{37}$$

where Δ_i denotes each triangle of wavevectors with maximum side length less than k_{comp}, and then integrate a χ^2 distribution from $\chi^2(k_{\text{comp}})$ to infinity to find an effective p-value indicating our confidence that the data are described well by our prediction.

In Fig. 4, we display the p-values corresponding to various fits of $B_{\text{EFT-1-loop}}$ as a function of k_{comp} on top and of k^3_{comp} on the bottom, as well as p-values for the EFT prediction including only the B_{c_s} counterterm, one-loop SPT, and the tree-level prediction. Comparing the $B_{\text{EFT-1-loop}}$ curves with different values of k_{max}, we see that overfitting is not an issue: even with the freedom of 3 arbitrary parameters, the fit cannot reach beyond $k_{\text{comp}} \sim 0.34h\,\text{Mpc}^{-1}$ before becoming much worse at low k. Therefore, this must be a region where a higher-order correction, namely $B_{\text{2-loop}}$ and associated counterterms, contributes significantly to the nonlinear bispectrum.

Furthermore, notice that the 3 extra counterterms are not able to improve the reach of the prediction into the UV more than about $\Delta k \sim 0.04h\,\text{Mpc}^{-1}$ as compared to the "B_{c_s}-only" curve. The ratio of $B_{\text{2-loop}}$ and $B_{\text{1-loop}}$ is expected to scale roughly like k/k_{NL} in this range, implying that if $B_{\text{2-loop}}$ is significant at $k \sim 0.34h\,\text{Mpc}^{-1}$, it will also be significant at $k \sim 0.3h\,\text{Mpc}^{-1}$, where the "$B_{c_s}$-only" prediction fails. Therefore, there is no regime in which the 3 extra counterterms are more important than $B_{\text{2-loop}}$, so it is self-consistent to neglect these 3 terms (we may still include B_{c_s}, though, because it is enhanced relative to the other counterterms by a factor of 2π) [6]. Indeed, as a

[6] This interpretation is further confirmed by the fact that the best fit values for the $c_{1,2,3}$ parameters giving rise to the red dotted line in the top of Fig. 4 are respectively equal to $c_1 = 0.39\,\text{Mpc}^2/h^2$, $c_2 = -5.51\,\text{Mpc}^2/h^2$, $c_3 = 8.48\,\text{Mpc}^2/h^2$. An equally good fit is obtained just using the B_{c_2} and B_{c_3} counterterms, whose have best fit values are $c_2 = -4.31\,\text{Mpc}^2/h^2$, $c_3 = 7.53\,\text{Mpc}^2/h^2$. These numbers are quite larger than what naively expected, even after considering the small normalization of the shapes of B_{c_2} and B_{c_3}. This further suggests that these counterterms

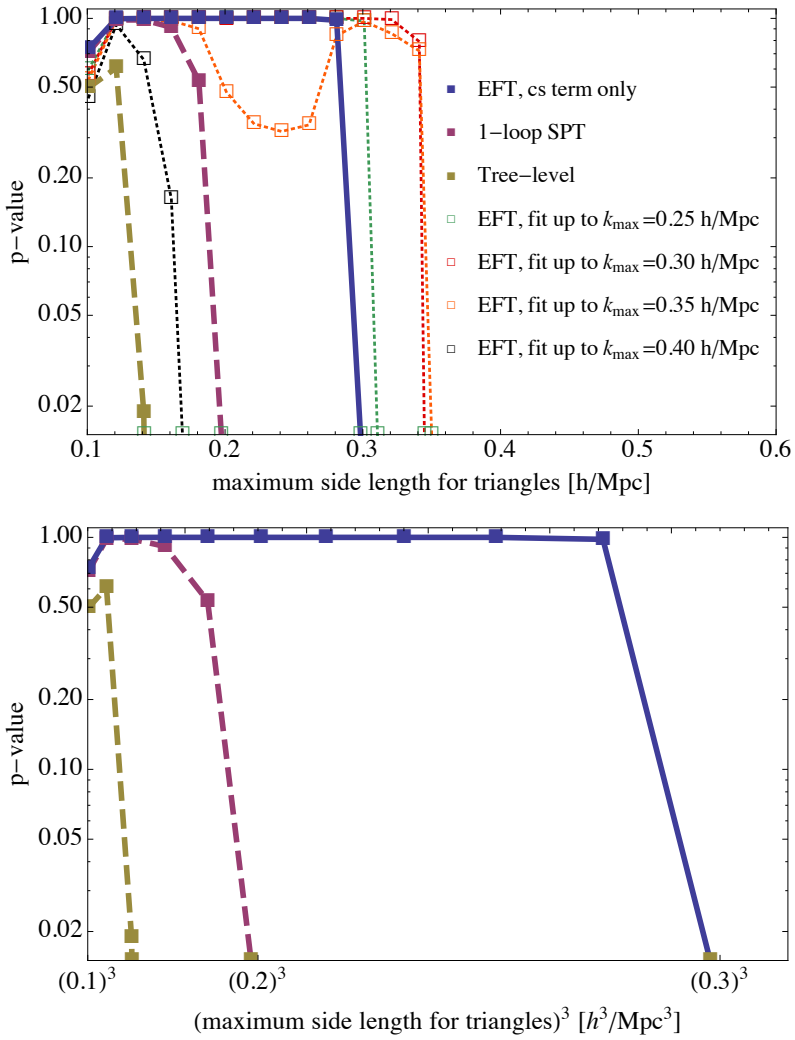

Figure 4: *Top: P-values corresponding to comparisons of various theory curves to nonlinear data, as described in the main text, as a function of the maximum side length of the triangles used to compute the p-value. Solid and dashed curves have no free parameters: they show in solid EFT at one loop (the $c^2_{s(1)}$ has been fixed by fitting the EFT prediction for the matter power spectrum), and in dashed SPT at one loop and SPT or EFT at tree level, while dotted curves represent the EFT prediction after adding the 3 free new counterterms that are fitted to nonlinear bispectrum data up to the maximum k indicated in the legend. Bottom: same as on top, but with $k^3_{\rm comp}$ on the x-axis. Since the number of available modes grows as $k^3_{\rm comp}$, the bottom plot gives a pictorial representation of the gain in information that is obtained by reaching higher k's.*

further confirmation of this, a scaling-universe estimate for $B_{c_1}/B_{\text{2-loop}}$ gives ~ 0.3 at $k \sim 0.3h\,\text{Mpc}^{-1}$,

are trying to compensate for the lack in the theoretical prediction of the 2-loop diagram, which is important in that k-range. Of course it would be nice to explicitly and more definitively verify this argument with an higher order calculation, something that we leave to future work.

which independently implies that the additional counterterms are not parametrically smaller than $B_{\text{2-loop}}$ in this region. We expect a similar contribution from the other counterterms [7] .

The resulting calculation, equivalent to one-loop SPT plus B_{c_s}, has *no* free parameters once c_s^2 is fixed by fitting to the matter power spectrum, and extends the range of the prediction compared to one-loop SPT by ∼50%, which corresponds to a factor of ∼3.5 more modes whose behavior is reliably captured by the theory. We summarize the shape of the bispectrum for dark matter that is valid up to $k \simeq 0.3h\,\text{Mpc}^{-1}$ from the EFTofLSS in Fig. 5.

More in detail, Figures 6, 7, and 8 display comparisons of various theory curves with the nonlinear data, which we have for isosceles triangles ($k_2 = k_1$) as well as configurations for which $k_2 = 1.5k_1$ and $k_2 = 2k_1$. There is some configuration-dependence in the maximum wavenumber up to which the EFT prediction can reliably reach, but the average limit of validity is around $k \sim 0.3h\,\text{Mpc}^{-1}$, similar to the reach of the one-loop prediction for the matter power spectrum. In addition, for equilateral triangles the "B_{c_s}-only" deviates from the data by around 25% at $k \sim 0.3h\,\text{Mpc}^{-1}$, as predicted (within $\mathcal{O}(1)$) by our prior estimate for B_{332}.

To compute the EFT predictions, we have used CAMB [13] to generate a linear power spectrum,

[7] This estimate follows from the following steps. First, based on Eq. (4), we find that for equilateral triangles,

$$B_{\text{tree}} \sim 3 \times 2 \times P_{11}(k)^2 \times \frac{2}{7} \,, \tag{38}$$

where the 2/7 comes from $F_2^{(\text{s})}$ in the equilateral limit. From Eq. (27), we then use

$$B_{c_1} \sim 3 \times 2c_1\, k^2 P_{11}(k)^2 \sim 6c_1\, k^2 \times \frac{7}{12} B_{\text{tree}} \,. \tag{39}$$

Comparing this with the estimate for B_{332} from Eq. (32), we find

$$\frac{B_{c_1}}{B_{\text{2-loop}}} \sim \frac{21}{16\pi^2} \frac{c_1\, k^2}{(k/k_{\text{NL}})^{2(3+n)}} \,. \tag{40}$$

We expect $c_1 \sim \bar{c}_1/(2\pi)$, and upon plugging this in, along with $\bar{c}_1 = 2.45\text{Mpc}^2/h^2$, $k_{\text{NL}} = 3.2h\,\text{Mpc}^{-1}$, and $n = -2.1$, we find a value of ∼0.3 at $k \sim 0.3h\,\text{Mpc}^{-1}$.

Notice the following important fact. The current universe can be approximated with the union of two power laws, the transition point being at $k_{\text{tr}} \simeq 0.25h\,\text{Mpc}^{-1}$ [8]. All our estimates so far have been focussed on the most UV region of our fit, where $n = -2.1$ and $k_{\text{NL}} \simeq 3.2h\,\text{Mpc}^{-1}$. For $k \lesssim k_{\text{tr}}$, the linear power spectrum is fitted with a power law with $n \simeq -1.7$ and $\tilde{k}_{\text{NL}} \sim 1.5h\,\text{Mpc}^{-1}$. Eq. (40) can be applied to k's below k_{tr} by using $\tilde{k}_{\text{NL}}$ and $n \simeq -1.7$, a slope which is quite steeper than -2.1. This means that, as we move towards the infrared, the importance of the additional counterterms relative to $B_{\text{2-loop}}$ grows, and one could potentially find oneself in the situation in which one is allowed to include the additional counterterms without including $B_{\text{2-loop}}$, because this is justified in some relatively IR region, while not being so in the most UV region. One can easily estimate that we are currently not in this situation for two concurrent reasons: first, by $k \simeq 0.1h\,\text{Mpc}^{-1}$, the ratio from (40) is still sensibly smaller than one; second, as we move to the IR, the numerical data have larger error bars that make the inclusion of the additional counterterms, as well as of the two-loop term, practically unnoticeable, even though their effect might be at percent level. This interpretation is verified by Figures 6, 7 and 8 below. This subtlety will become more apparent after we perform the two-loop computation, something that we plan to do in the next future, and when we will have more precise data. In particular, with precise enough data, we expect the fit to improve also at low k's below k_{tr}, after the inclusion of $B_{\text{2-loop}}$ and of the additional counterterms, a fact that with our available data is not measurable.

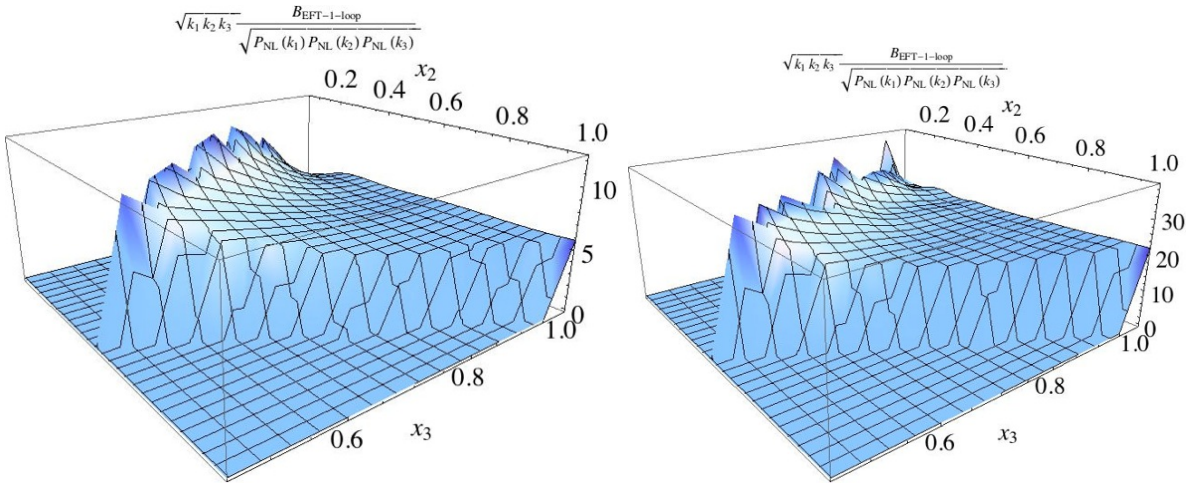

Figure 5: *The shape of the dark matter bispectrum given by the EFTofLSS, with* $k_1 = 0.1h\,Mpc^{-1}$ *on the left, and* $k = 0.3h\,Mpc^{-1}$ *on the right.*

and a version of the Copter code [17] modified to utilize the IR-safe integrands of [10] and Monte Carlo integration routines from the CUBA library [18], to compute $P_{\text{1-loop}}$ and $B_{\text{1-loop}}$.

4 Conclusions

In this paper we have studied the prediction for the equal-time bispectrum of dark matter at redshift $z = 0$ at one loop in the EFTofLSS. Since the equal time matter bispectrum is IR-safe, we have contented ourselves with not performing the IR-resummation of [7], which leaves us with a small residual $\sim 2\%$ oscillations that we will address in future work. Our main interest here was to study the UV reach of the prediction of the EFTofLSS. At one loop, the power spectrum at $z = 0$ agrees with numerical simulations at 1% up to $k \simeq 0.3h\,\text{Mpc}^{-1}$ [2] at one-loop and up to $k \simeq 0.6h\,\text{Mpc}^{-1}$ at two loops [8], after the IR-resummation has been performed [7]. This prediction requires us to fix a parameter, the so called speed of sound c_s^2, to account for the mistakes from the short distance physics that are accidentally included when doing perturbative calculations. When passing to the bispectrum, we have found that there is no need to include any additional parameter when performing the calculation at one loop. This is so because by the time the additional counterterms that could be inserted in the bispectrum calculation are computed, they contribute in a way that is not safely larger than the two-loop contribution that we do not compute. The only counterterm that we are justified to insert is the c_s term that had already appeared in the power spectrum calculation and had been measured from that observable. For this reason, without any additional parameter to fit, we find that the prediction of the EFTofLSS for the equal-time bispectrum of dark matter at $z = 0$ agrees very well with N-body simulations up to $k \simeq 0.3h\,\text{Mpc}^{-1}$, given the accuracy of the measurements, which

is of order a few percent at the highest k of interest [8]. This is a factor of 50% better than SPT [9]. While the fit is very good on average up to $k \simeq 0.3h\,\mathrm{Mpc}^{-1}$, the fit performs somewhat worse on equilateral configurations, failing approximately at $k \simeq 0.23h\,\mathrm{Mpc}^{-1}$, in agreement with expectations that for a given maximum k, equilateral triangles are more nonlinear than for the other shapes. We should also point out that the simulation we use has a σ_8 value which is about 10% higher than the current preferred value for our cosmology, so it is expectable that the comparison with observations or simulations with lower σ_8 or at higher redshifts will show an even better agreement. Still, given the large number of triangular configurations, the average reach of validity of the fit is $k \simeq 0.3h\,\mathrm{Mpc}^{-1}$.

This is a very promising result. The scale up to which we are able to match the data is quite comparable to the one up to which the EFTofLSS matches numerical data in the power spectrum at one loop. This is an important confirmation of the paradigm of the EFTofLSS, because it is expected that all quantities, when evaluated at the same order in perturbation theory, should match the numerical data to approximately the same wavenumber.

Additionally, it is quite remarkable that we can achieve our result without the addition of a new parameter. The value of c_s^2 is fitted to the power spectrum, and the prediction for the bispectrum follows without any freedom. In fact, we can even ask if the fit can be improved by adding additional quadratic counterterms to the calculation. This is a useful check because there is some uncertainty on the actual size of the various terms, so that it is possible that the additional quadratic counterterms might potentially contribute in a larger way than the two-loop contribution. We instead find that after adding the additional counterterms, the k-reach of the fit is improved only marginally, which shows that the two-loop contribution is relevant at the scales where our one-loop calculation fails. Somewhat contrary to what happens for the power spectrum, it is very straightforward to identify the k-value when the prediction of the EFT stops matching the data. Finally, we notice that the same c_s^2 parameter determined from the matter power spectrum was predicting the momentum power spectrum so that it agreed with the numerical data up to $k \simeq 0.3\,h\,\mathrm{Mpc}^{-1}$. In other words, the two-loop matter power spectrum, the one-loop momentum power spectrum, and now the one-loop bispectrum are all predicted with only one parameter.

There are a number of ways that we envision to proceed. First, it would be interesting to have more accurate N-body simulations, to tighten even more the error bars and understand better the performance of the prediction. Alternatively, and potentially even better, we could perform the EFT calculations directly for the actual realization being simulated by the codes, so that cosmic variance would be made negligible. Second, as it was done for the power spectrum, we would like to extend the calculation to two loops and include IR-resummation. These results obtained in the context of the EFTofLSS keep suggesting that there is a much larger number of cosmological modes that are amenable to analytic techniques. We believe this program is very important to assess what we will learn on primordial cosmology in the next decade, and therefore we are eager to push it forward.

[8] The error is dominated by the difference of the power spectrum used in the EFT calculation, where we used the realizations-averaged power spectrum, and the actual δ's simulated by the numerical code.

[9] The improvement at one loop with respect to SPT is less strong than in the power spectrum. This might be due to the fact that the relative weight of the counterterms with respect to the loops is diminished as we increase the number of external legs.

Acknowledgments

Raul E. Angulo and Marcel Schmittfull provided the measurement from the numerical simulations, while the other authors performed the analytic calculations in the EFT and the fits to the data.

We thank Simon White for a brief but intense conversation that helped motivating this project. We thank Daniel Green for initial collaboration. We thank Oliver Hahn, Eiichiro Komatsu, Uroš Seljak, Rashid Sunyaev and Matias Zaldarriaga for interesting conversations. S.F. is partially supported by the Natural Sciences and Engineering Research Council of Canada. L.S. is supported by DOE Early Career Award DE-FG02-12ER41854 and by NSF grant PHY-1068380.

Appendix

A Solving the Equations of Motion

In this appendix, we review the method to perturbatively solve the equations of motion for δ and v^i in the EFTofLSS, using the approximation that the time-dependence of each solution is given by an appropriate power of the linear growth factor $D_1(a)$ (normalized to unity at $a = 1$). If we wish to only make predictions for $z = 0$, it is acceptable to approximate the time-dependence in this way, since the error incurred by this approximation has been shown numerically to be very small [2].[10] In addition, since we only work up to one-loop order, any errors made by this approximation can be partially absorbed into the free parameters we fit to data.

A.1 Loop corrections and linear counterterms

We first review the solutions arising from the standard nonlinear terms ($\sim \delta\theta$ and $\sim \theta\theta$, where $\theta \equiv \partial_i v^i$) appearing in the equations of motion, as well as from the single linear counterterm ($\sim \partial^2\phi$) that has previously been considered in studies of the EFTofLSS, as it is the relevant counterterm for the matter power spectrum at one and two loops [2, 8]. We refer the reader to [8, 2] for a more extensive discussion of the motivations and assumptions underlying the formalism we present below.

The starting point is the equations of motion from [8], including only the term from the stress tensor that is linear in $\partial^2\phi$, integrated against an unknown kernel that parametrizes the non-locality

[10] A more thorough investigation of this point, as well as a formalism that allows computations to be carried out using the full time-dependence, can be found in [19].

in time of the coupling between long and short modes of the fields:

$$
\begin{aligned}
a\mathcal{H}\delta' + \theta &= -\int_{\boldsymbol{q}} \alpha(\boldsymbol{q}, \boldsymbol{k}-\boldsymbol{q})\delta(\boldsymbol{k}-\boldsymbol{q})\theta(\boldsymbol{q}) \ , \\
a\mathcal{H}\theta' + \mathcal{H}\theta + \frac{3}{2}\mathcal{H}_0^2\,\Omega_{\rm m}\frac{a_0^3}{a}\delta &= -\int_{\boldsymbol{q}} \beta(\boldsymbol{q}, \boldsymbol{k}-\boldsymbol{q})\theta(\boldsymbol{k}-\boldsymbol{q})\theta(\boldsymbol{q}) \\
&\qquad + \epsilon k^2 \int \frac{da'}{a'\mathcal{H}(a')}\kappa_1(a,a')\,[\partial^2\phi(\tau', \boldsymbol{x}_{\rm fl})]_{\boldsymbol{k}} \ , \qquad (41)
\end{aligned}
$$

where ϵ is a parameter inserted to organize the powers of $\kappa_1(a,a')$ appearing in the solutions we will derive, and where

$$
\alpha(\boldsymbol{k},\boldsymbol{q}) = \frac{(\boldsymbol{k}+\boldsymbol{q})\cdot\boldsymbol{k}}{k^2} \ , \qquad \beta(\boldsymbol{k},\boldsymbol{q}) = \frac{(\boldsymbol{k}+\boldsymbol{q})^2\,\boldsymbol{k}\cdot\boldsymbol{q}}{2q^2k^2} \ . \qquad (42)
$$

We use the labelled brackets $[f(\boldsymbol{x}_{\rm fl}(\boldsymbol{x}))]_{\boldsymbol{k}}$ to mean that we take the Fourier transform of the given function f and evaluate it at the momentum $\boldsymbol{k}$: $[f(\boldsymbol{x}_{\rm fl}(\boldsymbol{x}))]_{\boldsymbol{k}} \equiv \int d^3x\ e^{-i\boldsymbol{x}\cdot\boldsymbol{k}} f(\boldsymbol{x}_{\rm fl}(\boldsymbol{x}))$. We use $\boldsymbol{x}_{\rm fl} \equiv \boldsymbol{x}_{\rm fl}[\tau,\tau'] = \boldsymbol{x} - \int_{\tau'}^{\tau} d\tau''\boldsymbol{v}(\tau'', \boldsymbol{x}_{\rm fl}[\tau,\tau''])$ as the argument of ϕ to ensure that the equations of motion are diffeomorphism-invariant, and also because the behavior of a mode along its entire past trajectory could in principle have an influence on other modes. However, since we will only consider up to one-loop counterterms in this work, and the difference between $\boldsymbol{x}_{\rm fl}$ and $\boldsymbol{x}$ only becomes apparent in two- or higher-loop calculations, we can take $\boldsymbol{x}_{\rm fl} \approx \boldsymbol{x}$. We can also use Poisson's equation to rewrite $\partial^2\phi$ in terms of δ, transforming the second equation into

$$
\begin{aligned}
a\mathcal{H}\theta' + \mathcal{H}\theta + \frac{3}{2}\mathcal{H}_0^2\,\Omega_{\rm m}\frac{a_0^3}{a}\delta &= -\int_{\boldsymbol{q}} \beta(\boldsymbol{q}, \boldsymbol{k}-\boldsymbol{q})\theta(\boldsymbol{k}-\boldsymbol{q})\theta(\boldsymbol{q}) \\
&\qquad + \epsilon k^2 \int \frac{da'}{a'\mathcal{H}(a')}K(a,a')\delta(a',\boldsymbol{k}) \ , \qquad (43)
\end{aligned}
$$

where

$$
K(a,a') \equiv \frac{3}{2}H_0^2\,\Omega_{\rm m}\frac{a_0^3}{a'}\,\kappa_1(a,a') \ . \qquad (44)
$$

These equations can be solved using the following ansatz:

$$
\begin{aligned}
\delta(a,\boldsymbol{k}) &= \sum_{n=1}^{\infty}[D_1(a)]^n\delta^{(n)}(\boldsymbol{k}) + \epsilon\sum_{n=1}^{\infty}[D_1(a)]^{n+\zeta}\tilde{\delta}^{(n)}(\boldsymbol{k}) \ , \qquad (45) \\
\theta(a,\boldsymbol{k}) &= -\mathcal{H}(a)f\sum_{n=1}^{\infty}[D_1(a)]^n\theta^{(n)}(\boldsymbol{k}) - \epsilon\mathcal{H}(a)f\sum_{n=1}^{\infty}[D_1(a)]^{n+\zeta}\tilde{\theta}^{(n)}(\boldsymbol{k}) \ , \qquad (46)
\end{aligned}
$$

under the assumptions that $\delta^{(n)}(a',\boldsymbol{k}) = [D_1(a')/D_1(a)]^n\,\delta^{(n)}(a,\boldsymbol{k})$ and $\Omega_{\rm m}(a) \approx f^2$, where $f \equiv \partial\log D_1/\partial\log a$. (Recall that these assumptions allow us to solve for the momentum-dependent part of the solution at each order using recurrence relations that do not involve the time variable, as

explained in [8].) The $\boldsymbol{k}$-dependent parts of the solutions are written in terms of kernels F_n and G_n in the following manner:

$$\delta^{(n)}(\boldsymbol{k}) = \int_{\boldsymbol{q}_1} \cdots \int_{\boldsymbol{q}_n} (2\pi)^3 \delta_{\rm D}(\boldsymbol{k} - \boldsymbol{q}_{1\cdots n}) F_n(\boldsymbol{q}_1, \ldots, \boldsymbol{q}_n) \delta^{(1)}(\boldsymbol{q}_1) \cdots \delta^{(1)}(\boldsymbol{q}_n) \ , \tag{47}$$

$$\theta^{(n)}(\boldsymbol{k}) = \int_{\boldsymbol{q}_1} \cdots \int_{\boldsymbol{q}_n} (2\pi)^3 \delta_{\rm D}(\boldsymbol{k} - \boldsymbol{q}_{1\cdots n}) G_n(\boldsymbol{q}_1, \ldots, \boldsymbol{q}_n) \delta^{(1)}(\boldsymbol{q}_1) \cdots \delta^{(1)}(\boldsymbol{q}_n) \ , \tag{48}$$

with $\tilde{\delta}^{(n)}(\boldsymbol{k})$ and $\tilde{\theta}^{(n)}(\boldsymbol{k})$ written analogously in terms of $\tilde{F}_n$ and $\tilde{G}_n$. Once F_n, G_n, $\tilde{F}_n$, and $\tilde{G}_n$ are specified, then any correlation function of δ or θ can be calculated up to a specified order. The resulting expression will be in terms of the linear matter power spectrum, defined by

$$\left\langle \delta^{(1)}(\boldsymbol{k}) \delta^{(1)}(\boldsymbol{k}') \right\rangle = (2\pi)^3 \delta_{\rm D}(\boldsymbol{k} + \boldsymbol{k}') P_{11}(k) \ , \tag{49}$$

which is calculated numerically by a Boltzmann code such as CAMB [13] and used as an input to the EFTofLSS computation.

Plugging Eqs. (45) to (48) into the equations of motion and collecting terms of order ϵ^0 yields the following recurrence relations for F_n and G_n, familiar from SPT (e.g. [4]):

$$\begin{aligned} F_n(\boldsymbol{q}_1, \ldots, \boldsymbol{q}_n) &= \sum_{m=1}^{n-1} \frac{G_m(\boldsymbol{q}_1, \ldots, \boldsymbol{q}_m)}{(2n+3)(n-1)} \left[(2n+1) \frac{\boldsymbol{k} \cdot \boldsymbol{k}_1}{k_1^2} F_{n-m}(\boldsymbol{q}_{m+1}, \ldots, \boldsymbol{q}_n) \right. \\ &\qquad \left. + \frac{k^2 (\boldsymbol{k}_1 \cdot \boldsymbol{k}_2)}{k_1^2 k_2^2} G_{n-m}(\boldsymbol{q}_{m+1}, \ldots, \boldsymbol{q}_n) \right] , \\ G_n(\boldsymbol{q}_1, \ldots, \boldsymbol{q}_n) &= \sum_{m=1}^{n-1} \frac{G_m(\boldsymbol{q}_1, \ldots, \boldsymbol{q}_m)}{(2n+3)(n-1)} \left[3 \frac{\boldsymbol{k} \cdot \boldsymbol{k}_1}{k_1^2} F_{n-m}(\boldsymbol{q}_{m+1}, \ldots, \boldsymbol{q}_n) \right. \\ &\qquad \left. + n \frac{k^2 (\boldsymbol{k}_1 \cdot \boldsymbol{k}_2)}{k_1^2 k_2^2} G_{n-m}(\boldsymbol{q}_{m+1}, \ldots, \boldsymbol{q}_n) \right] . \end{aligned} \tag{50}$$

Meanwhile, the terms of order ϵ^1 (corresponding to solutions involving a single power of $K(a, a')$) give recurrence relations for $\tilde{F}_n$ and $\tilde{G}_n$, under the assumption that

$$c_n(a) = \bar{c}_n (\xi D_1(a)^\zeta \mathcal{H}^2 f^2) \ , \tag{51}$$

where

$$c_n(a) \equiv \int \frac{da'}{a' \mathcal{H}(a')} K(a, a') \frac{D_1(a')^n}{D_1(a)^n} \tag{52}$$

and ξ and ζ are constants. In [8], the values $\zeta = 2$ and $\xi = 9$ were used; this choice for ζ arises from the assumption that the coefficient of the $k^2 P_{11}$ counterterm in the matter power spectrum has the same time-dependence as $P_{\text{1-loop}}$, while the choice for ξ cancels factors of $1/9$ that would otherwise have appeared in the $\tilde{F}_n$ kernels. (Note that changing ξ simply redefines $\bar{c}_n$, so we are free to set ξ to a convenient value.) In Eq. (51), leaving ζ arbitrary allows for a more general time-dependence

of the $k^2 P_{11}$ counterterm in the power spectrum, as shown to be necessary in [19].[11] The resulting recurrence relations are the following:

$$\tilde{F}_n(\boldsymbol{q}_1,\ldots,\boldsymbol{q}_n) = \frac{1}{(n-1+\zeta)(n+\frac{3}{2}+\zeta)} \times \Big\{ -\xi \bar{c}_n\, k^2 F_n(\boldsymbol{q}_1,\ldots,\boldsymbol{q}_n) + \sum_{m=1}^{n-1} \big[(n+\tfrac{1}{2}+\zeta)\alpha(\boldsymbol{k}_1,\boldsymbol{k}_2)\mathcal{A}_m(\boldsymbol{q}_1,\ldots,\boldsymbol{q}_n) + \beta(\boldsymbol{k}_1,\boldsymbol{k}_2)\mathcal{B}_m(\boldsymbol{q}_1,\ldots,\boldsymbol{q}_n) \big] \Big\} \ , \quad (53)$$

$$\tilde{G}_n(\boldsymbol{q}_1,\ldots,\boldsymbol{q}_n) = \frac{1}{(n-1+\zeta)(n+\frac{3}{2}+\zeta)} \times \Big\{ -\xi (n+\zeta) \bar{c}_n\, k^2 F_n(\boldsymbol{q}_1,\ldots,\boldsymbol{q}_n) + \sum_{m=1}^{n-1} \big[\tfrac{3}{2}\alpha(\boldsymbol{k}_1,\boldsymbol{k}_2)\mathcal{A}_m(\boldsymbol{q}_1,\ldots,\boldsymbol{q}_n) + (n+\zeta)\beta(\boldsymbol{k}_1,\boldsymbol{k}_2)\mathcal{B}_m(\boldsymbol{q}_1,\ldots,\boldsymbol{q}_n) \big] \Big\} \ , \quad (54)$$

where

$$\mathcal{A}_m(\boldsymbol{q}_1,\cdots \boldsymbol{q}_n) \equiv \tilde{G}_m(\boldsymbol{q}_1,\ldots,\boldsymbol{q}_m) F_{n-m}(\boldsymbol{q}_{m+1},\ldots,\boldsymbol{q}_n) + G_m(\boldsymbol{q}_1,\ldots,\boldsymbol{q}_m) \tilde{F}_{n-m}(\boldsymbol{q}_{m+1},\ldots,\boldsymbol{q}_n) \ , \quad (55)$$

$$\mathcal{B}_m(\boldsymbol{q}_1,\cdots \boldsymbol{q}_n) \equiv \tilde{G}_m(\boldsymbol{q}_1,\ldots,\boldsymbol{q}_m) G_{n-m}(\boldsymbol{q}_{m+1},\ldots,\boldsymbol{q}_n) + G_m(\boldsymbol{q}_1,\ldots,\boldsymbol{q}_m) \tilde{G}_{n-m}(\boldsymbol{q}_{m+1},\ldots,\boldsymbol{q}_n) \ . \quad (56)$$

The value of ξ can be fixed by examining the lowest-order counterterm appearing in the matter power spectrum,

$$\left\langle \tilde{\delta}^{(1)}(\boldsymbol{k}) \delta^{(1)}(\boldsymbol{k}') \right\rangle = (2\pi)^3 \delta_{\rm D}(\boldsymbol{k}+\boldsymbol{k}') P^{(c_{\rm s})}_{\rm tree}(k) \ , \quad (57)$$

which involves $\tilde{F}_1(\boldsymbol{k})$:

$$\tilde{F}_1(\boldsymbol{k}) = -\frac{\xi}{\zeta(\zeta+\frac{5}{2})} \bar{c}_1 k^2 \ . \quad (58)$$

To simplify this expression, we set $\xi = \zeta(\zeta+5/2)$, implying that

$$P^{(c_{\rm s})}_{\rm tree}(k,a) = -2[D_1(a)]^{2+\zeta} \bar{c}_1 k^2 P_{11}(k) \ . \quad (59)$$

This explicitly shows the relationship between ζ and the time-dependence of the tree-level counterterm in the power spectrum.

[11] In a cosmological model in which loop corrections diverge (for example, a scaling universe with sufficiently high tilt), recall that the $k^2 P_{11}$ counterterm in the power spectrum will have two parts: one that depends on the method used to regulate the loop integrals, whose role is to cancel the regulator-dependence (e.g. Λ-dependence in the case of a hard momentum cutoff Λ) of the result, and another whose role is to capture the finite effects of the UV modes that have been "integrated out" of the theory. In the formalism presented here, this would be incorporated by splitting $K(a,a')$ into two separate functions $K_\Lambda(a,a')$ and $K_{\rm finite}(a,a')$, each associated with a different value of ζ and different perturbative solutions. For the realistic cosmology we consider in this paper, however, the loop corrections converge on their own and do not require a regulator, and so we only need to consider $K(a,a')$ and ζ corresponding to the finite counterterm.

Now, to fix the value of ζ, one can utilize the fact that over the range where we expect the one-loop EFT prediction for the power spectrum to be valid, $0.10h\,\mathrm{Mpc}^{-1} \lesssim k \lesssim 0.30h\,\mathrm{Mpc}^{-1}$, the linear power spectrum resembles that of a scaling universe with tilt $n \approx -1.7$. In such a universe, the equations of motion obey a scaling symmetry that uniquely determines the value of ζ to be $4/(3+n) \approx 3.1$, and this is also the value that results from a fit of the one-loop EFT prediction to nonlinear power spectra at different redshifts [19]. Therefore, in this paper we use $\zeta = 3.1$ in our numerical calculations. Also, dimensional analysis and the presence of a trivial angular integral in $P_{\text{1-loop}}$ determine the following relationship between $\bar{c}_1$ and the parameter we ultimately fit for, $c^2_{s(1)}$:

$$\bar{c}_1 = \frac{(2\pi)c^2_{s(1)}}{k^2_{\text{NL}}} \ . \tag{60}$$

As mentioned in Sec. 2.2, the $\tilde{\delta}$ solutions contribute to two counterterms (displayed in Eq. (22) for $z = 0$) to the bispectrum, arising from the correlators of the form $\langle\tilde{\delta}^{(2)}(\boldsymbol{k}_1)\delta^{(1)}(\boldsymbol{k}_2)\delta^{(1)}(\boldsymbol{k}_3)\rangle$ and $\langle\tilde{\delta}^{(1)}(\boldsymbol{k}_1)\delta^{(2)}(\boldsymbol{k}_2)\delta^{(1)}(\boldsymbol{k}_3)\rangle$ (plus permutations of external momenta). The second one involves $\tilde{F}_1$ and $F_2^{(\text{s})}$, while the first one involves $\tilde{F}_2^{(\text{s})}$, which takes the form

$$\begin{aligned}
-(1+\zeta)(7+2\zeta)\tilde{F}_2^{(\text{s})}(\boldsymbol{k}_1,\boldsymbol{k}_2) = \bar{c}_1 \Bigg\{ &\left(5 + \frac{113\zeta}{14} + \frac{17\zeta^2}{7}\right)(k_1^2 + k_2^2) + \left(7 + \frac{148\zeta}{7} + \frac{48\zeta^2}{7}\right)\boldsymbol{k}_1\cdot\boldsymbol{k}_2 \\
&+ \left(2 + \frac{59\zeta}{7} + \frac{18\zeta^2}{7}\right)\left(\frac{1}{k_1^2} + \frac{1}{k_2^2}\right)(\boldsymbol{k}_1\cdot\boldsymbol{k}_2)^2 + \left(\frac{7}{2} + \frac{9\zeta}{2} + \zeta^2\right)\left(\frac{k_1^2}{k_2^2} + \frac{k_2^2}{k_1^2}\right)\boldsymbol{k}_1\cdot\boldsymbol{k}_2 \\
&+ \left(\frac{20\zeta}{7} + \frac{8\zeta^2}{7}\right)\frac{(\boldsymbol{k}_1\cdot\boldsymbol{k}_2)^3}{k_1^2 k_2^2} \Bigg\}
\end{aligned} \tag{61}$$

in the local-in-time limit of $K(a,a')$ (for which $\bar{c}_n = \bar{c}_1$ for all n). In the nonlocal case, extra factors of $\bar{c}_2$ will appear in $\tilde{F}_2^{(\text{s})}(\boldsymbol{k}_1,\boldsymbol{k}_2)$, but unless the nonlocality is very severe, $\bar{c}_2$ will be very close to $\bar{c}_1$ (see [8] for a more precise statement, involving parameterizing the nonlocality by the power of the growth factor $D_1(a')$ appearing in $K(a,a')$).

A.2 Quadratic counterterms

As mentioned in Sec. 2.2, the linear term in $(\partial\tau)_{\rho_l}{}^i$ does not exhaust the possible tree-level counterterms that can enter into the bispectrum calculation—there are also three independent quadratic terms consistent with symmetries that can be written down, along with one linear combination of fields that only contributes at quadratic and higher order:

$$\partial_i(\partial\tau)_{\rho_l}{}^i \supset \partial^2\delta^2 + \partial^2\left[\frac{\partial^j\partial^k}{\partial^2}\delta\cdot\frac{\partial_j\partial_k}{\partial^2}\delta\right] + \partial_i\left[\frac{\partial^i\partial^j}{\partial^2}\delta\cdot\partial_j\delta\right] + \partial^2\left[\frac{\theta}{-\mathcal{H}(a)f} - \delta\right] \ . \tag{62}$$

Taking the Fourier transform of each term and inserting into the Euler equation in the same way as for the linear term, we obtain the following:

$$
\begin{aligned}
&a\mathcal{H}\theta' + \mathcal{H}\theta + \frac{3}{2}\mathcal{H}_0^2\,\Omega_{\rm m}\frac{a_0^3}{a}\delta \\
&\quad = -\int_{\boldsymbol{q}} \beta(\boldsymbol{q},\boldsymbol{k}-\boldsymbol{q})\theta(\boldsymbol{k}-\boldsymbol{q})\theta(\boldsymbol{q}) + k^2\int\frac{da'}{a'\mathcal{H}(a')}K(a,a')\delta(a',\boldsymbol{k}) \\
&\qquad + \int\frac{da'}{a'\mathcal{H}(a')}\left\{K_1(a,a')\,k^2\int_{\boldsymbol{q}}\delta(a',\boldsymbol{q})\delta(a',\boldsymbol{k}-\boldsymbol{q})\right. \\
&\qquad\qquad + K_2(a,a')k^2\int_{\boldsymbol{q}}\frac{[\boldsymbol{q}\cdot(\boldsymbol{k}-\boldsymbol{q})]^2}{q^2|\boldsymbol{k}-\boldsymbol{q}|^2}\delta(a',\boldsymbol{q})\delta(a',\boldsymbol{k}-\boldsymbol{q}) \\
&\qquad\qquad + K_3(a,a')\int_{\boldsymbol{q}}\frac{1}{2}\boldsymbol{q}\cdot(\boldsymbol{k}-\boldsymbol{q})\left[\frac{\boldsymbol{k}\cdot\boldsymbol{q}}{q^2}+\frac{\boldsymbol{k}\cdot(\boldsymbol{k}-\boldsymbol{q})}{|\boldsymbol{k}-\boldsymbol{q}|^2}\right]\delta(a',\boldsymbol{q})\delta(a',\boldsymbol{k}-\boldsymbol{q}) \\
&\qquad\qquad \left. + K_4(a,a')\,k^2\left[\frac{\theta(a',\boldsymbol{k})}{-\mathcal{H}(a')f}-\delta(a',\boldsymbol{k})\right]\right\}\ . \qquad (63)
\end{aligned}
$$

Notice that when Eqs. (45) and (46) are inserted into the last (K_4) term, the contents of the square brackets have the same time-dependence at each order.

In principle, from here we could repeat the procedure from App. A.1, deriving solutions analogous to $\tilde{\delta}^{(n)}$ for each of the four new terms shown above. However, in this work we are only interested in tree-level counterterms (for which each δ will be evaluated on the linear solution $\delta^{(1)}$) evaluated at $z=0$, for which the time-dependence has no effect. Therefore, we can simply read off the new second-order contributions to $\delta(a=1,\boldsymbol{k})$ from the equation above:

$$
\begin{aligned}
\delta(a=1,\boldsymbol{k})_{\rm counterterm} = -\int_{\boldsymbol{q}}\left\{c_1k^2 + c_2\,k^2\frac{[\boldsymbol{q}\cdot(\boldsymbol{k}-\boldsymbol{q})]^2}{q^2|\boldsymbol{k}-\boldsymbol{q}|^2} + c_3\,\frac{1}{2}\boldsymbol{q}\cdot(\boldsymbol{k}-\boldsymbol{q})\left[\frac{\boldsymbol{k}\cdot\boldsymbol{q}}{q^2}+\frac{\boldsymbol{k}\cdot(\boldsymbol{k}-\boldsymbol{q})}{|\boldsymbol{k}-\boldsymbol{q}|^2}\right]\right. \\
\left. + c_4\,k^2\Big[G_2^{(\rm s)}(\boldsymbol{q},\boldsymbol{k}-\boldsymbol{q}) - F_2^{(\rm s)}(\boldsymbol{q},\boldsymbol{k}-\boldsymbol{q})\Big]\right\}\delta^{(1)}(\boldsymbol{q})\delta^{(1)}(\boldsymbol{k}-\boldsymbol{q})\ . \qquad (64)
\end{aligned}
$$

Then, by taking the correlation of each term in Eq. (64) with two other linear δ solutions and symmetrizing over external momenta, we obtain the counterterms listed in Eqs. (27). For example, B_{c_1} is obtained from

$$
(2\pi)^3\delta_{\rm D}(\boldsymbol{k}_1+\boldsymbol{k}_2+\boldsymbol{k}_3)B_{c_1}(k_1,k_2,k_3) = \left\langle -c_1k_1^2\int_{\boldsymbol{q}}\delta^{(1)}(\boldsymbol{q})\delta^{(1)}(\boldsymbol{k}_1-\boldsymbol{q})\delta^{(1)}(\boldsymbol{k}_2)\delta^{(1)}(\boldsymbol{k}_3)\right\rangle + 2\ \text{perms}\ . \qquad (65)
$$

B Divergences and Renormalization in Scaling Universes

In this appendix we want to illustrate that in scale-free universes where the linear power spectrum is given by a power law

$$
P_{11}(k) = \frac{1}{k_{\rm NL}^3}\left(\frac{k}{k_{\rm NL}}\right)^n\ , \qquad (66)
$$

the one-loop power spectrum and bispectrum present UV divergences. These divergences should, and indeed we show that they can, be cancelled by a suitable chosen combination of the counterterms we have included in the EFT. These are the usual linear $c^2_{s(1)}$ counterterm, as well as the three new quadratic ones. This result can be interpreted as a sufficient condition that the EFT counterterms are present and induced by the short distance fluctuations. Notice that it is a sufficient but not necessary condition, as even if the counterterms were not needed to cancel any UV divergence, they would still be allowed on symmetry grounds. Furthermore this calculation can be seen as a further check, together with the verification that IR divergences cancel, that our algebra is correct.

Notice that in a scaling universe, the time dependence of the EFT parameters is completely determined by the scaling symmetry present in these universes. The finite part and the UV divergent part, which represents the proper counterterm, as it literally counters a loop diagram, have different time dependences. In particular, the time dependence of the UV divergent part must be exactly the same as the one of the divergent loops. Since in this section we are interested in showing that the UV divergences can be cancelled, we focus only on the UV divergent part of the counterterms. We will consider only the $n = -1$ case, which has just a logarithmic divergence. Higher n's will have additional subleading divergences that will be very similarly cancelled by higher derivative counterterms that we do not study here.

We start by noticing that the one-loop power spectrum is divergent, the divergence coming from the P_{13} diagram. This requires a renormalization by using the $c^2_{s(1)}$ counterterm, as described in general in [2] and for scaling universes in [21, 10]. We obtain

$$\bar{c}_1 = -\frac{122\pi}{315}\frac{1}{k^2_{\rm NL}}\log\left(\frac{\Lambda}{k_{\rm min}}\right) \ , \tag{67}$$

where as in (60) we have that $\bar{c}_1 = \frac{2\pi}{k^2_{\rm NL}} c^2_{s(1)}$. Here we take the parameter $\zeta = 2$ as we are interested in canceling the UV divergent part of the one-loop diagrams.

Next we move to the Bispectrum. The divergent part is given by:

$$\begin{aligned} B_{\text{1-loop,UV}} = &-\frac{\pi}{169785 k_1^3 k_2^3 k_3^3 k_{\rm NL}^6}\log\left(\frac{\Lambda}{k_{\rm NL}}\right) \times \\ &\left(12409k_1^9 + 29479k_1^7\left(k_2^2+k_3^2\right) - 11461k_1^6\left(k_2^3+k_3^3\right) + k_1^5\left(-30427k_2^4 + 104866k_2^2k_3^2 - 30427k_3^4\right)\right. \\ &+k_1^4\left(-30427k_2^5 + 11461k_2^3k_3^2 + 11461k_2^2k_3^3 - 30427k_3^5\right) - 11461k_1^3\left(k_2^2-k_3^2\right)^2\left(k_2^2+k_3^2\right) \\ &\left.+k_1^2\left(29479k_2^7 + 104866k_2^5k_3^2 + 11461k_2^4k_3^3 + 11461k_2^3k_3^4 + 104866k_2^2k_3^5 + 29479k_3^7\right) + \right. \\ &(k_2-k_3)^2(k_2+k_3) \\ &\qquad \left.\times\left(12409k_2^6 + 12409k_2^5k_3 + 54297k_2^4k_3^2 + 42836k_2^3k_3^3 + 54297k_2^2k_3^4 + 12409k_2k_3^5 + 12409k_3^6\right)\right) . \end{aligned} \tag{68}$$

Simple algebra show that the divergent part can be written as a linear combination of our three quadratic counterterms in (27) plus the $c^2_{s(1)}$ counterterm in (21), all evaluated with $\zeta = 2$. We obtain

$$-B_{\text{1-loop, UV}}(k_1,k_2,k_3) = c_1\, B_{c_1}(k_1,k_2,k_3) + c_2 B_{c_2}(k_1,k_2,k_3) + c_3 B_{c_3}(k_1,k_2,k_3) \ .$$

where

$$c_1 = \frac{892\pi}{56595}\frac{1}{k_{\rm NL}^2}\log\left(\frac{\Lambda}{k_{\rm min}}\right), \quad c_2 = \frac{2914\pi}{33957}\frac{1}{k_{\rm NL}^2}\log\left(\frac{\Lambda}{k_{\rm min}}\right), \quad c_3 = \frac{27998\pi}{52595}\frac{1}{k_{\rm NL}^2}\log\left(\frac{\Lambda}{k_{\rm min}}\right) . \tag{69}$$

This completes our demonstration that the UV divergences can be reabsorbed.

C A Simplification to the IR Resummation

In [7] it was shown that the IR-resummed expression for the dark matter power spectrum up to order N in $\epsilon_{\delta<}$ was given by a convolution integral of the following form

$$P_{\delta\delta}(k;t_1,t_2)|_N = \sum_{j=0}^{N}\int \frac{d^3k'}{(2\pi)^3}\, M_{||_{N-j}}(k,k';t_1,t_2)\, P_{\delta\delta,\,j}(k';t_1,t_2) , \tag{70}$$

where $P_{\delta\delta,\,j}(k';t_1,t_2)$ is the power spectrum evaluated to order j expanding both in $\epsilon_{\delta<}$ and $\epsilon_{s<}$. Here the convolution matrix M is given by

$$M_{||_{N-j}}(k,k';t_1,t_2) = \int d^3r\, d^3q\, P_{||_{N-j}}(\vec{r}|\vec{q};t_1,t_2)\, e^{i\vec{k}\cdot\vec{r}}\, e^{-i\vec{k}'\cdot\vec{q}} , \tag{71}$$

with $P_{||_{N-j}}(\vec{r}|\vec{q};t_1,t_2)$ is related to the probability for a particle of starting at position $\vec{q}$ and ending up at position $\vec{r}$:

$$P_{||_{N-j}}(\vec{r}|\vec{q};t_1,t_2) = \int \frac{d^3k''}{(2\pi)^3}\, e^{-i\vec{k}''\cdot(\vec{q}-\vec{r})}\, F_{||_{N-j}}(\vec{q},\vec{k}'';t_1,t_2) , \tag{72}$$

where $F_{||_{N-j}}$ is defined in eq. (43) of [7]. In [7], M was evaluated from (71) for every k and k' by performing a bi-dimensional Fast Fourier Transform (FFT). It is however possible to alternatively evaluate M by performing, for each k of interest, a one-dimensional FFT. This can be seen by plugging (72) into (71). The $\vec{r}$ integral can be done leading to a $(2\pi)^3\delta_{\rm D}(\vec{k}''+\vec{k})$, which in turns allows us to evaluate the $\vec{k}''$ integral. We then obtain

$$M_{||_{N-j}}(k,k';t_1,t_2) = \int d^3q\, F_{||_{N-j}}(\vec{q},-\vec{k};t_1,t_2)\, e^{i(\vec{k}-\vec{k}')\cdot\vec{q}} . \tag{73}$$

Plugging (73) into (70), we can then perform then angular $\vec{k}'$ integrals analytically, leaving

$$P_{\delta\delta}(k;t_1,t_2)|_N = \sum_{j=0}^{N}\int dk'\, \hat{M}_{||_{N-j}}(k,k';t_1,t_2)\, P_{\delta\delta,\,j}(k';t_1,t_2) , \tag{74}$$

where

$$\hat{M}_{||_{N-j}}(k,k';t_1,t_2) = \frac{1}{2\pi^2}\int d^3q\, \frac{k'\sin(k'q)}{q}\, e^{i\vec{k}\cdot\vec{q}}\, F_{||_{N-j}}(\vec{q},\vec{k};t_1,t_2) , \tag{75}$$

and where we used that $F_{||_{N-j}}(\vec{q},-\vec{k};t_1,t_2) = F_{||_{N-j}}(\vec{q},\vec{k};t_1,t_2)$. The angular $\vec{q}$ integrals can also be performed analytically, leaving a single q integral in (75) that can then be evaluated via an FFT at each desired k value, after which the remaining k' integral in (74) is trivial to carry out numerically.

It is also possible to re-derive this expression working from the derivation presented [7]. We can start from eq. (44) of [7], that reads:

$$P_{\delta\delta}(k_1;t_1,t_2)|_N = \int d^3q\; e^{-i\vec{k}_1\cdot\vec{q}} \sum_{j=0}^{N} \left[F_{||_{N-j}}(\vec{q},\vec{k}_1;t_1,t_2)\cdot K(\vec{q},\vec{k}_1;t_1,t_2)_j\right] \;, \tag{76}$$

where $K(\vec{q},\vec{k}_1;t_1,t_2)_j$ is such that the power spectrum to order j expanding both in $\epsilon_{\delta<}$ and $\epsilon_{s<}$ is given by

$$P_{\delta\delta}(k;t_1,t_2)_j = \int d^3q\; e^{i\vec{k}\cdot\vec{q}}\; K(\vec{q},-\vec{k};t_1,t_2)_j \;. \tag{77}$$

It is useful to manipulate the above expression by multiplying by 1 written as

$$1 = \int \frac{d^3k_1'}{(2\pi)^3}\,(2\pi)^3\delta_{\rm D}(\vec{k}_1'-\vec{k}_1) = \int \frac{d^3k_1'}{(2\pi)^3}\int d^3q'\; e^{i\,\vec{q}'\cdot(\vec{k}_1'-\vec{k}_1)} \;, \tag{78}$$

so that, by exchanging $\vec{k}_1$ with $\vec{k}_1'$ when useful, we can write

$$\begin{aligned} &P_{\delta\delta}(k_1;t_1,t_2)\rangle|_N \\ &\quad= \sum_{j=0}^{N}\int \frac{d^3k_1'}{(2\pi)^3}\left[\int d^3q'\; e^{i\cdot(\vec{k}_1'-\vec{k}_1)\cdot\vec{q}'}\; F_{||_{N-j}}(\vec{q},\vec{k}_1;t_1,t_2)\right]\cdot\left[\int d^3q\; e^{-i\vec{k}_1'\cdot\vec{q}} K(\vec{q},\vec{k}_1';t_1,t_2)_j\right] \end{aligned} \tag{79}$$

Now, as done in [7], we perform the approximation to replace $F_{||_{N-j}}(\vec{q},\vec{k}_1;t_1,t_2) \to F_{||_{N-j}}(\vec{q}',\vec{k}_1;t_1,t_2)$, as this amounts to doing a mistake proportional to the gradient of the IR displacements. We therefore obtain directly eq. (70), but with the matrix M directly in the form (73).

D Consistency Check using Other Simulations

As a check on our primary results presented in Sec. 3.3, we have also performed the same procedure on a second, independent set of simulations. These simulations are based on three realizations with $L_{\rm box} = 1600h^{-1}$Mpc and 512^3 grid points, assuming a flat ΛCDM model with $\Omega_{\rm b}h^2 = 0.0226$, $\Omega_{\rm c}h^2 = 0.11$, $\Omega_\Lambda = 0.734$, $h = 0.71$, $\Delta^2_{\mathcal{R}}(k_0) = 2.43\times10^{-9}$, and $n_{\rm s}(k_0) = 0.963$, where $k_0 = 0.002{\rm Mpc}^{-1}$; more details can be found in [20]. These cosmological parameters give, over the range $0.25h\,{\rm Mpc}^{-1} \lesssim k \lesssim 0.60h\,{\rm Mpc}^{-1}$, $P_{11}(k) \approx \frac{(2\pi)^3}{k_{\rm NL}^3}\left(\frac{k}{k_{\rm NL}}\right)^n$ with $n \approx -2.1$ and $k_{\rm NL} \approx 4.45h\,{\rm Mpc}^{-1}$.

The matter bispectrum we compare to was reconstructed from these simulations using an expansion of separable basis functions (see [20]), rather than the more traditional methods described in Sec. 3.1, and for this reason, the error estimate in Eq. (29) cannot be straightforwardly applied.

Instead, we expect there to be two main contributions to the errorbars: scatter between the three realizations, which can be used as a rough estimate for the cosmic variance, and the fact that we truncate the series of basis functions after a finite number of terms, which introduces a separate systematic error. We estimate the uncertainty incurred by this truncation—specifically, the difference between the exact $B_{\rm nonlinear}$ and the $B_{\rm nonlinear}$ reconstructed from the basis functions—by calculating this difference for $B_{\rm tree}$, for which we know the exact function. We then estimate the total uncertainty in our measurements of $B_{\rm nonlinear}$ by adding this truncation uncertainty, double the scatter between realizations (we double the measured scatter because three realizations will generally not correctly estimate the cosmic variance, and so we prefer to overestimate it), and an extra 2% systematic error. This is a rather gross estimate of the errorbars, but is still useful as a visual aide to determine whether the theoretical predictions are a reasonable match to the data. However, different triangles will have errors that are highly correlated, since the error on each triangle will arise from combined errors on the measured coefficients of each function in the separable basis, and the reader should keep in mind that we ignore these correlations in our fits and plots.

From there, we follow the same procedure as in Secs. 3.2 and 3.3. Fitting the one-loop EFT prediction to the matter power spectrum yields

$$c^2_{s(1)} = (2.33 \pm 0.06) \times \frac{1}{2\pi} \left(\frac{k_{\rm NL}}{h\,{\rm Mpc}^{-1}} \right)^2 \qquad (1\text{-}\sigma), \tag{80}$$

and we use this value, plus values of c_1, c_2, and c_3 obtained by fitting the one-loop bispectrum formula to all bispectrum triangles with maximum side length less than $0.3h\,{\rm Mpc}^{-1}$, to obtain the results shown in Figures 9, 10, and 11. Once again, the improvement of the EFT prediction over one-loop SPT is evident. The fact that such improvement occurs for two separate sets of simulations demonstrates that the improvement arises from properties of the EFTofLSS, rather than the details of any particular simulation.

References

[1] P. A. R. Ade *et al.* [BICEP2 Collaboration], "BICEP2 I: Detection Of B-mode Polarization at Degree Angular Scales," [arXiv:1403.3985] [astro-ph.CO].

[2] J. J. M. Carrasco, M. P. Hertzberg and L. Senatore, "The Effective Field Theory of Cosmological Large Scale Structures," JHEP **1209**, 082 (2012) [arXiv:1206.2926] [astro-ph.CO].

[3] D. Baumann, A. Nicolis, L. Senatore and M. Zaldarriaga, "Cosmological Non-Linearities as an Effective Fluid," JCAP **1207**, 051 (2012) [arXiv:1004.2488] [astro-ph.CO].

[4] F. Bernardeau, S. Colombi, E. Gaztanaga and R. Scoccimarro, "Large scale structure of the universe and cosmological perturbation theory," Phys. Rept. **367**, 1 (2002) [astro-ph/0112551].

[5] M. Crocce and R. Scoccimarro, "Renormalized cosmological perturbation theory," Phys. Rev. D **73** (2006) 063519 [astro-ph/0509418].

[6] R. A. Porto, L. Senatore and M. Zaldarriaga, "The Lagrangian-space Effective Field Theory of Large Scale Structures," [arXiv:1311.2168] [astro-ph.CO].

[7] L. Senatore and M. Zaldarriaga, "The IR-resummed Effective Field Theory of Large Scale Structures," [arXiv:1404.5954] [astro-ph.CO].

[8] J. J. M. Carrasco, S. Foreman, D. Green and L. Senatore, "The Effective Field Theory of Large Scale Structures at Two Loops," [arXiv:1310.0464] [astro-ph.CO].

[9] R. Scoccimarro, S. Colombi, J. N. Fry, J. A. Frieman, E. Hivon and A. Melott, "Nonlinear evolution of the bispectrum of cosmological perturbations," Astrophys. J. **496**, 586 (1998) [astro-ph/9704075].

[10] J. J. M. Carrasco, S. Foreman, D. Green and L. Senatore, "The 2-loop matter power spectrum and the IR-safe integrand," [arXiv:1304.4946] [astro-ph.CO].

[11] S. M. Carroll, S. Leichenauer and J. Pollack, "A Consistent Effective Theory of Long-Wavelength Cosmological Perturbations," [arXiv:1310.2920] [hep-th].

[12] R. E. Angulo, V. Springel, S. D. M. White, A. Jenkins, C. M. Baugh and C. S. Frenk, "Scaling relations for galaxy clusters in the Millennium-XXL simulation," MNRAS **426**, 2046 (2012) [arXiv:1203.3216] [astro-ph.CO].

[13] A. Lewis, A. Challinor and A. Lasenby, "Efficient computation of CMB anisotropies in closed FRW models," Astrophys. J. **538**, 473 (2000) [astro-ph/9911177].

[14] J. N. Fry, A. L. Melott and S. F. Shandarin, "The three-point correlation function in an ensemble of three-dimensional simulations," Astrophys. J. **412**, 504 (1993).

[15] H. A. Feldman, N. Kaiser and J. A. Peacock, "Power spectrum analysis of three-dimensional redshift surveys," Astrophys. J. **426**, 23 (1994) [astro-ph/9304022].

[16] R. Scoccimarro, E. Sefusatti and M. Zaldarriaga, "Probing primordial non-Gaussianity with large-scale structure," Phys. Rev. D **69**, 103513 (2004) [astro-ph/0312286].

[17] J. Carlson, M. White and N. Padmanabhan, "A critical look at cosmological perturbation theory techniques," Phys. Rev. D **80**, 043531 (2009) [arXiv:0905.0479] [astro-ph.CO].

[18] T. Hahn, "CUBA: A Library for multidimensional numerical integration," Comput. Phys. Commun. **168**, 78 (2005) [hep-ph/0404043v2].

[19] S. Foreman and L. Senatore, "Time-Dependence in the Effective Field Theory of Large-Scale Structures," to appear.

[20] M. M. Schmittfull, D. M. Regan and E. P. S. Shellard, "Fast estimation of gravitational and primordial bispectra in large scale structures," Phys. Rev. D **88**, 063512 (2013) [arXiv:1207.5678] [astro-ph.CO].

[21] E. Pajer and M. Zaldarriaga, "On the Renormalization of the Effective Field Theory of Large Scale Structures," JCAP **1308** (2013) 037 [arXiv:1301.7182] [astro-ph.CO].

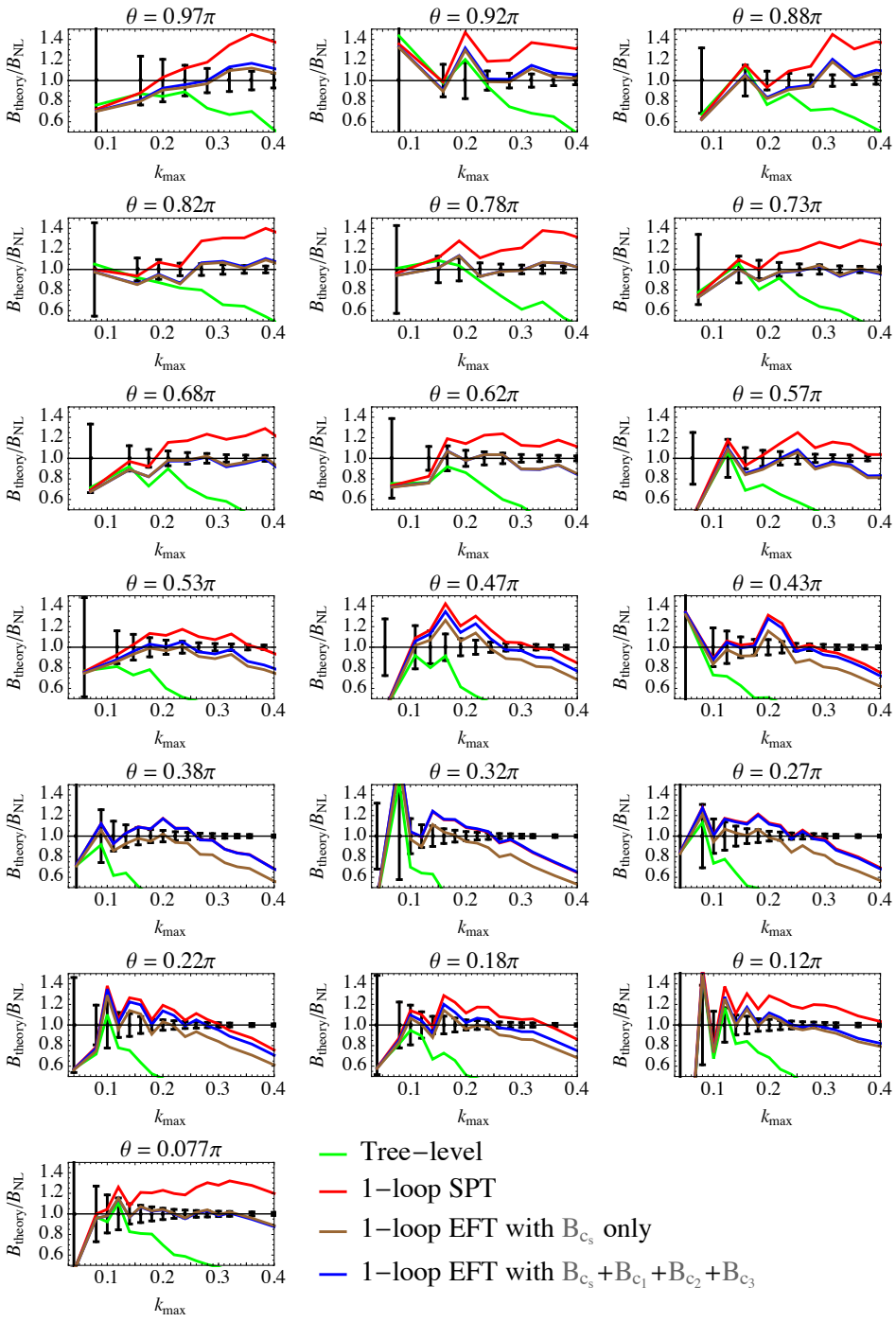

Figure 6: *Comparison of various theory curves, normalized to nonlinear bispectrum data for isosceles triangles ($k_2 = k_1$). The blue curve is fit using all triangles with maximum side length less than $0.3h\,Mpc^{-1}$. The EFT prediction fails at lower k on equilateral configurations than on flat or squeezed triangles, but on average, agreement with the errorbars is obtained for $k \lesssim 0.3h\,Mpc^{-1}$, even when no free parameters are fit to the bispectrum data.*

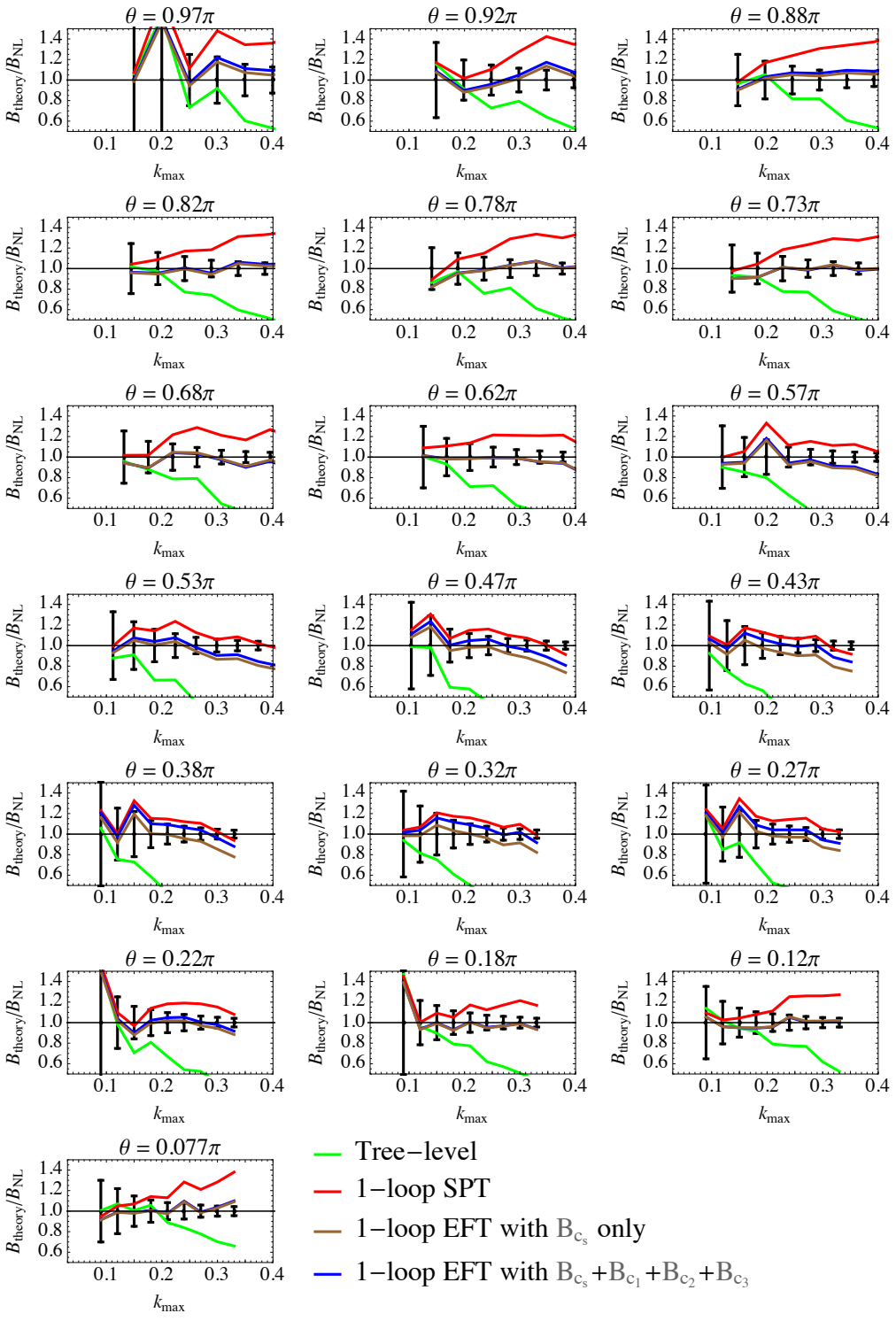

Figure 7: *As Fig. 6, but for triangles with* $k_2 = 1.5k_1$.

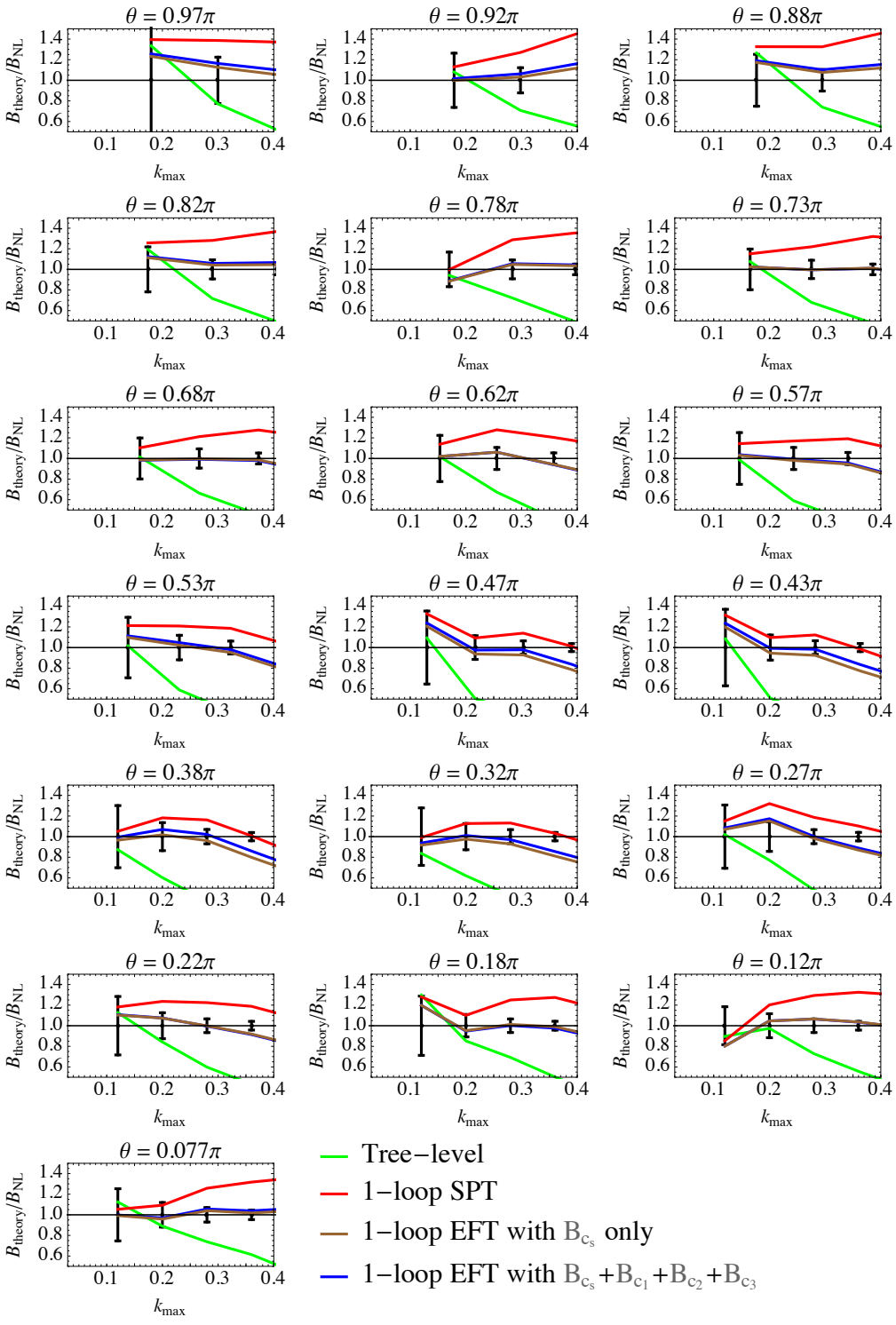

Figure 8: *As Fig. 6, but for triangles with* $k_2 = 2k_1$.

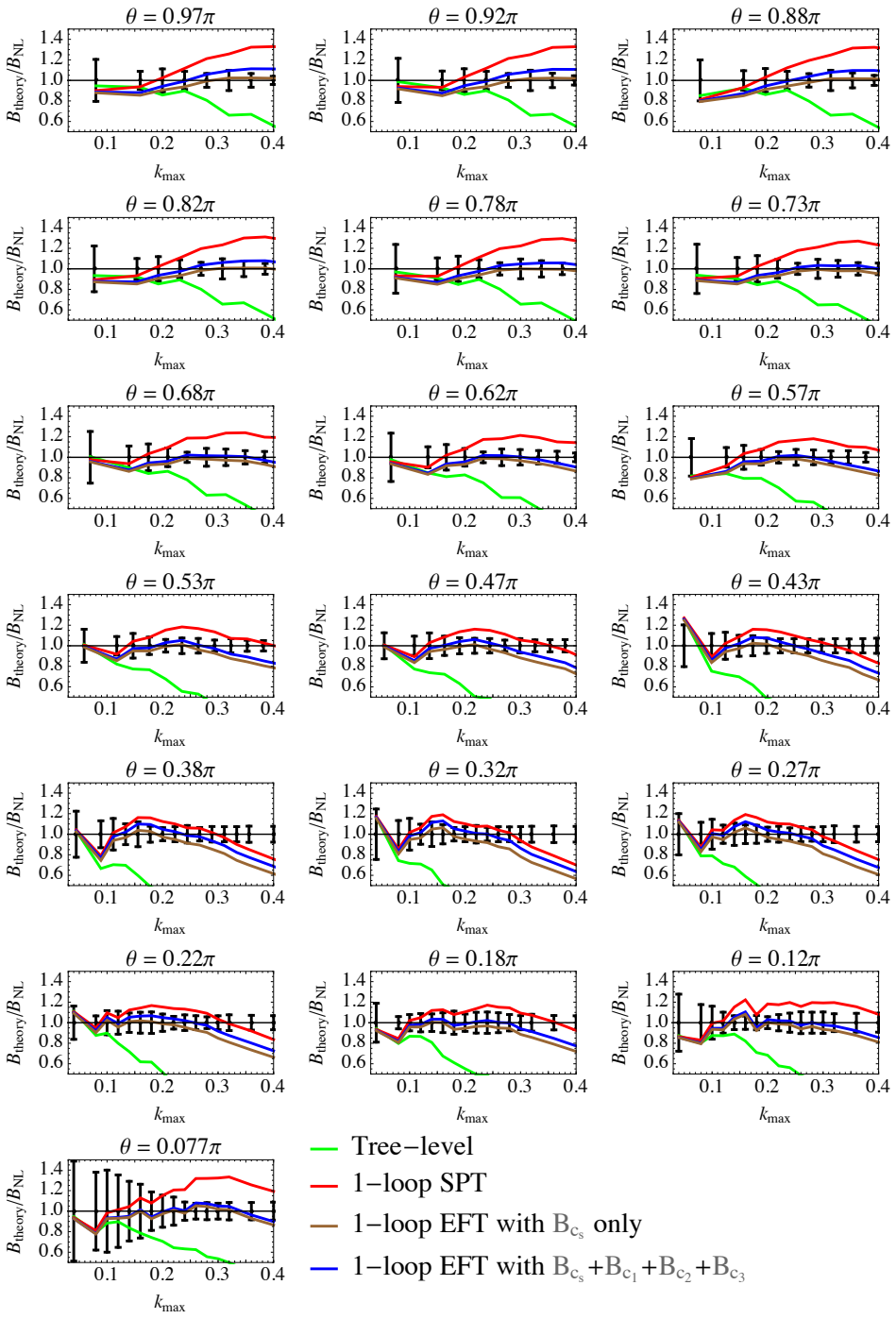

Figure 9: *Comparison of various theory curves, normalized to nonlinear bispectrum data for isosceles triangles ($k_2 = k_1$) measured from the simulations in App. D. The blue curve is fit using all triangles with maximum side length less than $0.3h\,Mpc^{-1}$. It is clear that the EFT predictions significantly improve upon the tree-level and SPT predictions, particularly for squeezed and flat configurations.*

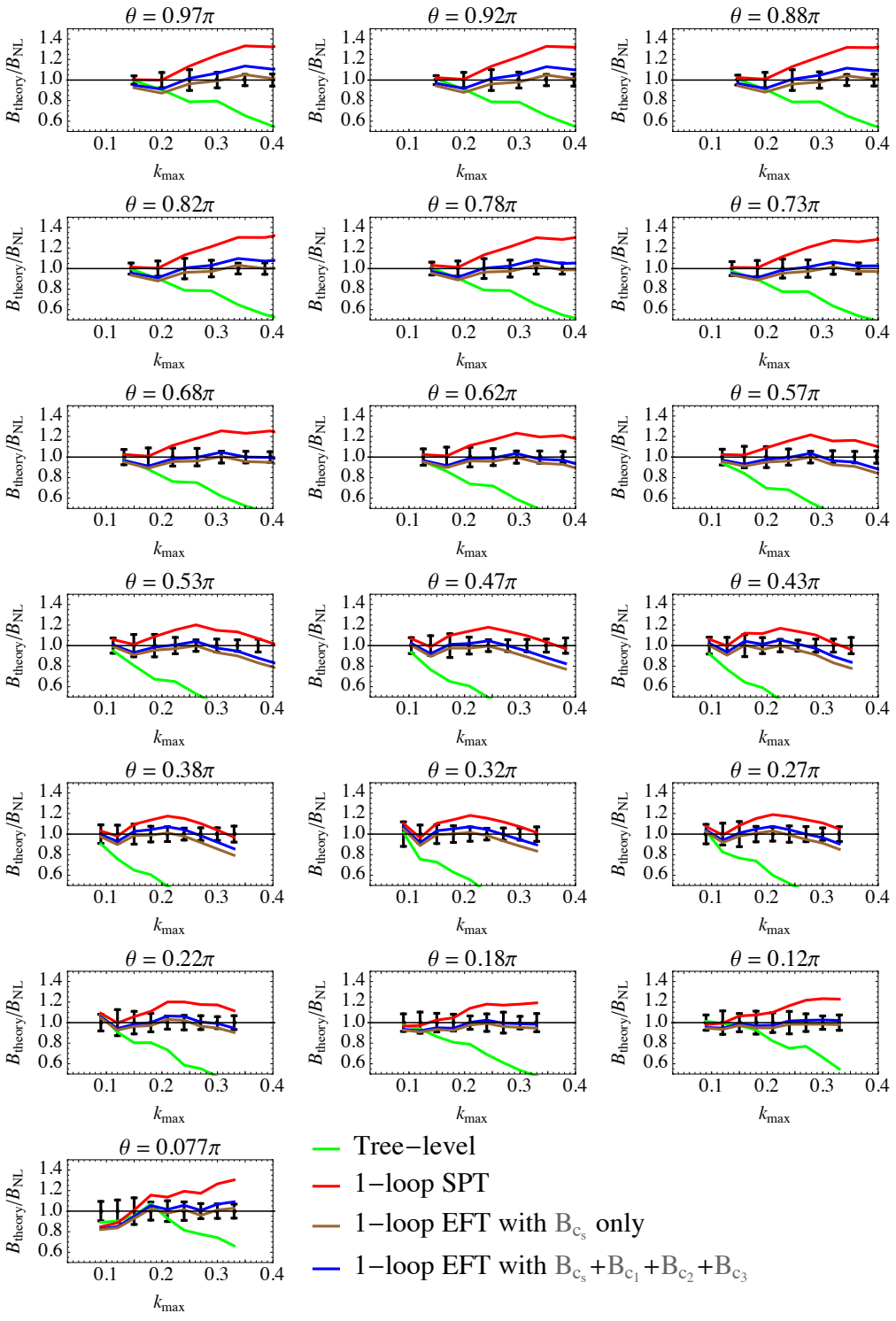

Figure 10: *As Fig. 9, but for triangles with* $k_2 = 1.5k_1$.

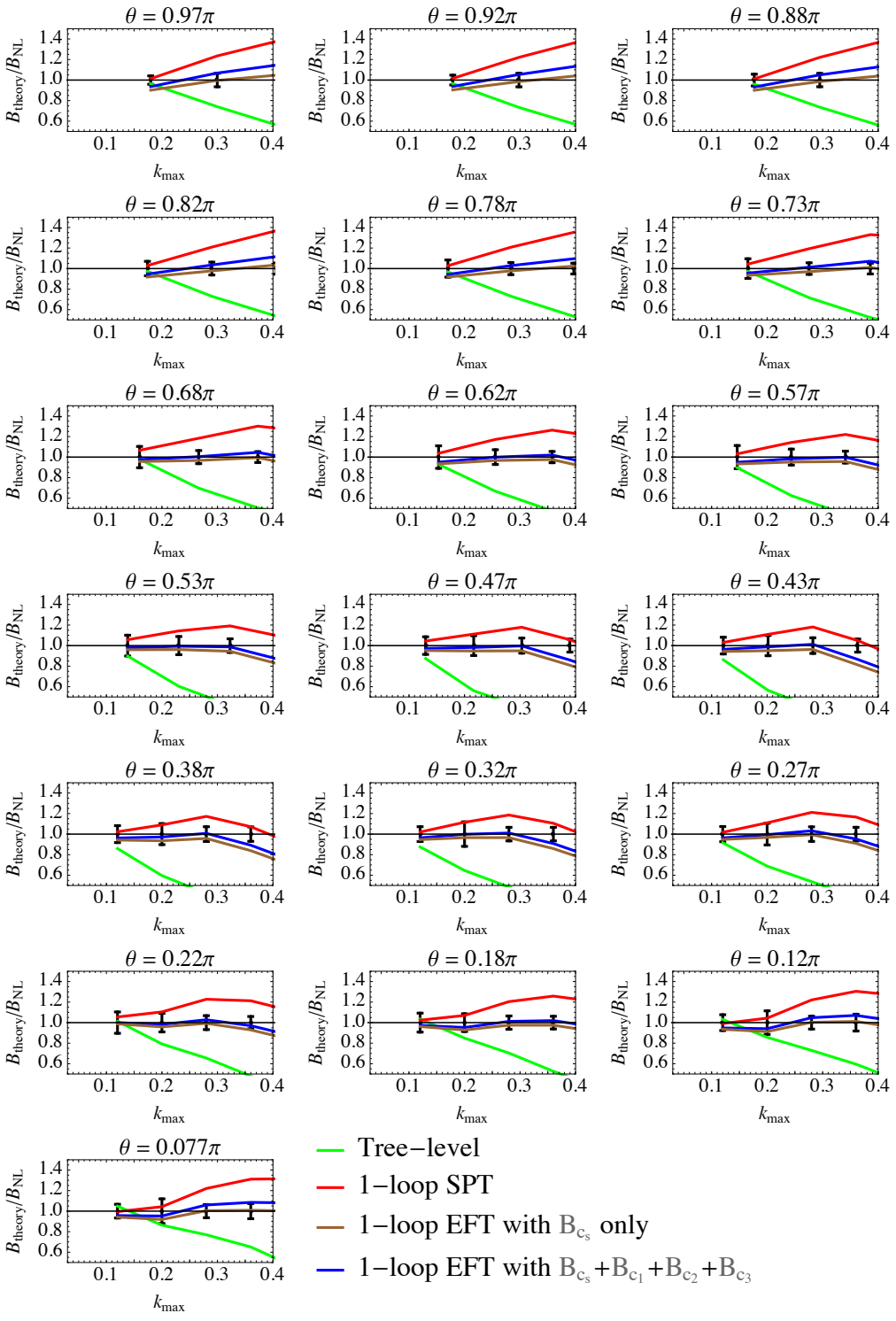

Figure 11: *As Fig. 9, but for triangles with* $k_2 = 2k_1$.